1968

A Calculation of Electron-Bremsstrahlung Produced in Thick Targets

Chris Gross
College of William & Mary - Arts & Sciences

A CALCULATION OF ELECTRON-BREMSSTRAHLUNG PRODUCED IN THICK TARGETS

A Thesis

Presented to

The Faculty of the Department of Physics

The College of William and Mary in Virginia

In Partial Fulfillment

of the Requirements for the Degree of

Master of Arts

By

Chris Gross

May 1968

APPROVAL SHEET

This thesis is submitted in partial fulfillment of

the requirements for the degree of

Master of Arts

Chris Gross

Author

Approved, May 1968

Herbert O. Funsten

Herbert O. Funsten, Ph.D.

Robert E. Welsh

Robert E. Welsh, Ph.D.

Arden Sher

Arden Sher, Ph.D.

APPROVAL SHEET

This thesis is submitted in partial fulfillment of the requirements for the degree of Master of Arts

Chris Gross
Author

Approved, May 1968

Herbert O. Funsten, Ph.D.

Robert E. Welsh, Ph.D.

Arden Sher, Ph.D.

ACKNOWLEDGEMENT

The author wishes to express his gratitude to the National Aeronautics and Space Administration for the opportunity to write this thesis. The author is especially grateful to Dr. Jag J. Singh for suggesting this thesis problem and for his many helpful discussions which were essential to the completion of this work.

TABLE OF CONTENTS

LIST OF TABLES

LIST OF FIGURES

Figure Page

ABSTRACT

Computer calculations of the bremsstrahlung intensity, differential in photon energy and angle, resulting from electrons of initial energy from .5 to 3.0 MeV being stopped in thick targets of several atomic numbers have been made. In this calculation the Bethe-Heitler formula corrected for atomic screening and the Sauter-Fano high-frequency limit formula were used to predict the bremsstrahlung cross sections for the electrons as they are brought to rest in the target. The electron distribution in the thick target was determined through the use of a Monte Carlo type calculation which utilized the multiple-scattering theory of Goudsmit and Saunderson. The effect of the fluctuation in $\frac{dE}{dx}$ on the electron distribution was also included. The calculated intensities compared favorably with experimental data for electron-bremsstrahlung produced in thick aluminum, iron, and gold targets.

A CALCULATION OF ELECTRON-BREMSSTRAHLUNG PRODUCED THICK TARGETS

INTRODUCTION

High energy electrons in passing through matter lose a portion of their kinetic energy in radiative interactions with the atomic nuclei and atomic electrons. In these radiative interactions, the kinetic energy lost by the electrons is in the form of photon emission known as bremsstrahlung. The intensity of the bremsstrahlung radiation produced per incident electron depends primarily on the atomic number of the target material and the electron energy. Bremsstrahlung can constitute a significant source of secondary radiation and the calculation of its intensity is often required in conjunction with background determinations and shielding studies.

Calculations of bremsstrahlung production for thin targets, e.g. a target whose thickness is such that electrons traversing it lose no appreciable energy by ionization, suffer no significant elastic deflections and have only one radiative collision, may be made from cross section formulas derived by Sommerfeld (ref. 1) for nonrelativistic electron energies and by Bethe and Hielter (ref. 2) and others (see ref. 3) for relativistic electron energies. Analytic formulas do not exist for the intermediate electron energy range where the Born approximation is not expected to be valid; however, numerical calculations, although very tedious, can be made to obtain the cross section values (ref. 4).

For the important practical case of a thick target where the electron's energy and direction is significantly affected and multiple radiative collisions may occur, analytic or empirical formulas are very

scarce as well as highly approximate in nature. The derivation of analytic thick target bremsstrahlung formulas have not been possible because of the complex mathematical form of both the thin target cross section formulas and the electron energy and angular distribution functions in a thick target. The only general approach available for calculating thick target bremsstrahlung intensities with reasonably reliable results is a numerical calculation based on the elementary processes occurring during the progress of an electron through the thick target. Because of the complexity of a numerical calculation of this type and the scarcity of experimental data with which to compare the results, only a few such calculations were made before 1962 (ref. 5 and 6).

With the discovery of the earth's trapped radiation field where intense regions of high energy electrons exist and with the advent of manned space flight into these regions, a new emphasis has been placed on the thick target bremsstrahlung problem. The dose from bremsstrahlung radiation must be accurately known to assess its potential biological hazard to man. The necessity to determine these doses has prompted the National Aeronautics and Space Administration to sponsor several experimental and theoretical studies of the thick target bremsstrahlung problem.

Under these NASA sponsored studies, theoretical calculations and experimental measurements of the angular distribution, spectral distribution, and total intensity of bremsstrahlung produced from electrons passing through thick targets have been made. The

theoretical calculations are based on various approximations and idealizations of the elementary processes involved in thick target bremsstrahlung production and have been made by both numerical integration and Monte Carlo techniques. The results of both calculational techniques have been in fair quantitive agreement with the experimental results for the electron energies and target materials with which they have been compared. The region of poorest agreement has been the lower and upper extremes of the photon energy spectrum. The reason for poor agreement of theory and experiment for this region can in part be traced back to the approximations used in describing the elementary processes.

It is the purpose of this study to make numerical calculations of thick target bremsstrahlung produced by electrons of 0.5 MeV, 1.00 MeV, 2.00 MeV, 2.8 MeV, and 3.0 MeV which take in account more accurately the elementary processes involved and to compare the results of these calculations to the experimental values recently measured by W. E. Dance and co-workers at the LTV Research Center, Dallas, Texas.

CHAPTER I

REVIEW OF PREVIOUS WORK

General analytic expressions for thick target bremsstrahlung intensities have not been derived owing principally to the inability to represent thin target bremsstrahlung formulas in simple analytical terms and to the complex distribution of electrons in both energy and angle in a thick target. The only analytic expression derived from theoretical considerations for thick target bremsstrahlung is the formula due to Krammer (ref. 7), and this formula predicts only the bremsstrahlung spectral distribution. Also, since the formula is based on nonrelativistic theory, its application is severely limited. For electrons whose kinetic energies are on the order of and greater than the electron rest mass energy, numerical calculations are the only recourse presently available, aside from empirical formulas, for calculating the angular distribution, spectral distribution, and total intensity of thick target bremsstrahlung production.

Several numerical calculations have been made during the last decade. In each of these calculations, various simplifications and approximations have been made in order to carry out a numerical evaluation of thick target bremsstrahlung intensities. It is attempted below to list the method and approximations made by each investigator in his calculation. The review, however, will be limited to electron energies representative of those in the earth's trapped radiation field and, therefore, not cover calculations for extremely

relativistic electron energies.

The first calculations of the spectral distributions at discrete angles of thick target bremsstrahlung for moderately relativistic electron energies were made by Miller, Motz, and Cialella (ref. 5). These calculations were made for 1.4 MeV electrons striking a thick tungsten target. The bremsstrahlung spectral intensities were calculated for photon energies from .4 to 1.4 MeV at angles of 0° and 90° with respect to the incident electron beam. The intensity of the photons per unit energy interval at energy k per steradian at angle φ per incident electron, $I(k, \phi)$, was estimated from the integral

$$I(k,\phi) = \int_{k+l}^{T_o} \int_{0}^{2\pi} \int_{0}^{\pi} N_A \left\{ 1 - B(E) \right\} N_e(E,\epsilon,\psi)\, \sigma_r(E,k,\theta) \sin\epsilon\, d\epsilon\, d\psi \frac{ds}{dE} dE \qquad (1.01)$$

where T_o is the total energy of the incident electron, N_A the number of target atoms per cubic centimeter, B(E) corresponds to the fractional number of electrons of energy E which have been backscattered out of the target, $N_e(E, \epsilon, \psi)$ represents the angular distribution of electron velocities as a function of electron energy, $\sigma_r(E, k, \theta)$ the differential bremsstrahlung cross section, dE/ds the stopping power, and the angles ϕ, θ, ψ, and ϵ are defined in figure 1. The derivation of the integral is quite straight forward. The expression

$$\{ 1 - B(E) \}\, N_e(E,\epsilon,\psi) \sin\epsilon\, d\epsilon\, d\psi$$

gives the probability that an electron whose energy has been reduced from its incident value T_o to E in passing through the target is traveling in the direction defined by angles ϵ and ψ, and the differential cross section $\sigma_r(E, k, \theta)$ give the probability per target atom that an electron of energy E will emit a photon of energy k

in the direction defined by θ, The number of target atoms encountered by the electron in the energy interval between E and E + dE is given by $N_A \frac{ds}{dE} dE$. The integrand of equation (1.01) therefore gives the probability that a photon of energy k will be emitted in the direction ϕ as a function of the electron's energy and direction. By integrating over the energy and angles of the electron as it is brought to rest in the target, the total probability for emission of a photon of energy k in the direction ϕ per incident electron per steridian or the intensity $I(k, \phi)$ is obtained.

By expanding the angular distributions of electrons and the bremsstrahlung cross sections in terms of Legendre polynomials as

$$N_e(E,\epsilon) = \frac{1}{4\pi} \sum_{\ell} f_\ell(E) P_\ell(\cos\epsilon) \tag{1.02}$$

$$\sigma_r(E,k,\theta) = \frac{\sigma_r(E,k)}{4\pi} \sum_{m} g_m(E,k) P_m(\cos\theta) \tag{1.03}$$

Equation (1.01) may be integrated over its angular variables and yields

$$I(k,\phi) = \frac{N_A}{2} \int_{k+1}^{T_o} \left\{1-B(E)\right\} \frac{\sigma_r(E,k)}{4\pi} \sum_{\ell=0}^{\infty} \frac{2}{2\ell+1} f_\ell(E)\, g_\ell(E,k)\, P_\ell(\cos\phi) \frac{ds}{dE} dE \tag{1.04}$$

In evaluating equation (1.04), the Bethe-Heitler bremsstrahlung cross section formula was approximated by $\sigma_r(E, k) = 11.5 \left[1-k/(E-1)\right]$, which the authors estimate to be good to about 5% from .4 to 1.4 MeV, the multiple scattering theory of Goudsmit and Saunderson was used to evaluate multiple scattering effects, the energy straggling was neglected, the stopping power was estimated from the Bloch formula and assumed constant from .4 to 1.4 MeV, and the fractional number of back-scattered electrons was taken from experimental data. With these

approximations, equation (1.04) was evaluated for photon energies from .4 to 1.4 MeV at 0° to 90°.

A comparison of the results predicated by equation (1.04) and the measured bremsstrahlung intensities at 0° and 90° is shown in figure 2. The theoretical values in this figure have been corrected for photon attenuation in the tungsten target and surrounding medium. The measured and theoretical curves show that the energy distribution and the relative intensities of the radiation at these angles are in qualitative agreement. However, the absolute intensities indicated by the measured curves are about a factor of two greater than the theoretically predicted values. The authors believe the discrepancy arises primarily because the Bethe-Heitler bremsstrahlung formula underestimates the bremsstrahlung cross section for electrons in this energy range.

A recent calculation has been made by Scott (ref. 8) of the angular distribution of bremsstrahlung for electrons of about the same energy as that of Miller et al for thick aluminum and iron targets. Scott's formulation of the problem is analogous with that of Miller et al with exception that the photon attenuation and build-up in the target, and a correction for electron-electron bremsstrahlung is included. In this calculation the photon intensity $I(k, \phi)$ was computed by numerical evaluating on a high-speed electronic computer the triple integral

$$I(k,\phi)=(1+\tfrac{1}{Z})(1-R)\int_{k+1}^{T_0}\int_0^{2\pi}\int_0^{\pi} N_A B e^{-\mu_m t_x/\cos\phi} N_e(E,\epsilon,\psi)\,\sigma_r(E,k,\theta)\sin\epsilon\, d\epsilon\, d\psi \frac{ds}{dE} dE \qquad (1.05)$$

where k, ϵ, ψ, N_A, E, $N_e(E, \epsilon, \psi)$, E, $\sigma_r(E, k, \theta)$ and dE/ds have the same meaning as defined earlier and $(1 + \frac{1}{Z})$ is the electron-electron

bremsstrahlung correction factor, B and u_m the build-up and attenuation coefficients respectivity for photons of energy k, t_x the perpendicular target thickness that an electron of energy E has to penetrate to leave the target, and R the fraction of backscatter electrons. Since the factor (1-R) is not included under the integral signs, backscattering is taken into account only in a very approximate manner in this formulation.

In evaluating this integral, the exact form of the unscreened Bethe-Heitler cross section formula (equation 2BN, ref. 3) was used; the Goudsmit-Saunderson multiple scattering theory was evaluated for a screened, Rutherford scattering cross section, neglecting energy straggling and radiative collisions; the stopping power was estimated from the Bethe formula; and electron backscattering values, the photon attenuation and build-up coefficients were taken from experimental data.

The calculated values obtained from equation (1.05) are compared to the experimentally measured bremsstrahlung intensities of Dance, et al (ref. 9) for aluminum and iron at 0° and 30° for 1.0 MeV electrons in figures 3a and 3b. A better comparison between the theoretical and measured intensities is obtained for these targets and electron energy than those obtained by Miller et al for tungsten. The closer agreement of theoretical and experimental intensities arise not from the inclusion of electron-electron bremsstrahlung, photon attenuation and photon build-up or from the use of the exact form of Bethe-Heitler cross section and Bethe stopping power formula, but most likely from a better estimate of the bremsstrahlung cross section by the Bethe-Heitler

formula for the lower atomic numbers.

Scott has also made a calculation of the photon spectrum integrated over all photon angles (ref. 10). The photon intensity, I(k), was obtained from the integral

$$I(k) = \int_{k+1}^{T_o} N_A \sigma_r(E,k) e^{-u_m(k)t_x} \frac{ds}{dE} dE \qquad (1.06)$$

where T_o, E, k, ds/dE, $u_m(k)$, and t_x have their previously defined meaning and $\sigma_r(E, k)$ is the unscreened Bethe-Heitler formula integrated over all photon directions. A comparison of results predicted by equation (1.06) and experimental results of Dance et al for 1 MeV electron incident on a thick aluminum target is shown in figure 4. The calculated and experimental results compare quite favorably with only small deviations at high and low photon energies.

A different approach to the problem of calculating thick target bremsstrahlung intensities has been taken by Berger and Seltzer (ref. 11). Instead of an integral formulation, a Monte Carlo technique has been used to calculate the angular and spectral distributions of the bremsstrahlung intensities from thick targets. A combination of electron and photon Monte Carlo programs were used in order to take into account correctly the motion of the electron prior to producing bremsstrahlung, and scattering and absorption of the bremsstrahlung photons before emerging from a target in the shape of a slab formed by two infinite planes. The incident electron direction was taken to be perpendicular to the slab.

The electron part of the calculation was done by a reduced random walk Monte Carlo model based on the Goudsmit-Saunderson multiple scattering theory and the continuous-slowing-down approximation. The photon part involves a random sampling with the use of the method of expected values and the unscreened Bethe-Heitler bremsstrahlung cross section formula empirically corrected. The calculation ignores electron energy straggling, Compton electrons and pair electrons, and bremsstrahlung in turn produced by these particles.*

Comparisons of the theoretical intensities obtained from the Monte Carlo calculation and experimentally measured intensities at 15° are shown in figures 5a and 5b for .5 and 2.0 MeV electrons respectively incident on thick aluminum targets. The comparisons are, in general, quite good except for the low photon energy extreme.

In summary, the calculations of Miller et al are in qualitative agreement with the experimental results they obtained for 1.4 MeV electrons striking a thick tungsten target. However, the measured intensity was a factor of two greater than the calculated theoretical value. The discrepancy is explained on the basis that the Bethe-Heitler formula underestimates the thin target bremsstrahlung cross section for electrons in this energy range. Scott's calculations are in better quantitative agreement than those of Miller et al for 1 MeV electrons striking thick aluminum and iron targets. The agreement is

*More recent calculations by Berger do include these effects; however, they do not substantially improve the agreement of the calculated and measured bremsstrahlung intensity at the extreme ends of the photon energy spectrum.

is best for the intermediate photon energies and discrepancies are noted at both the lower and higher photon energy extremes. Both Miller et al and Scott integrated over all electron angles and energy to obtain the bremsstrahlung intensities. Berger's Monte Carlo results are in quite good agreement with experimental values except at the lower photon energy extreme.

CHAPTER II

COMBINATION INTEGRATION - MONTE CARLO APPROACH TO THICK TARGET BREMSSTRAHLUNG PROBLEM

The calculations reviewed in the last chapter indicate that both the integration and Monte Carlo approaches to the thick target bremsstrahlung problem give reasonable good results over a considerable part of the spectrum. The primary differences between the two calculations are as follows: (1) the Monte Carlo calculation incorporates electron backscattering from the target in the electron transport theory, while in the integration calculation backscattering must be allowed for by a separate experimentally determined multiplicative factor to correct the multiple scattering theory; (2) The perpendicular distance the electron has penetrated into the target, which is necessary to know to properly take in account photon attenuation, may be computed in the Monte Carlo calculation, while the path length which is not necessarily the perpendicular distance of penetration must be used in the integral calculation. If the backscattering data was accurate, the path length equal to the perpendicular electron penetration distance, results obtained from the integral formulation would be identical to those of the Monte Carlo treatment for an infinite number of electrons striking the target. The primary disadvantage of the Monte Carlo calculation is the amount of computer time necessary for calculating a spectrum with reasonable statistical accuracy. A single spectrum (containing 19 points from 0° to 180°

in steps of 10°) calculated by the Monte Carlo technique takes about 30 minutes while an integration calculation takes only about 15 seconds on an IBM 7094 computer.

The largest single source of error in the calculations discussed probably arises from the use of the unscreened Bethe-Heitler cross section formula. Experimental results for thin targets indicate that the unscreened Bethe-Heitler formula overestimates the cross section for low photon energies and underestimates the cross section for high photon energies. The inaccuracies are due to screening effects and failure of the Born approximation at the low and high photon energies, respectively. Other errors are introduced by neglecting the effect of radiative collisions on the stopping power and electron distribution, and the secondary effects of bremsstrahlung from Compton and pair electrons.

Theoretically, it would be possible to take in account all of the processes involved in thick target bremsstrahlung production, but to do so exactly would present a calculational problem of such magnitude that it would be unsolvable because of the practical considerations of computer speed and storage. It is possible, however, to include some of the processes that were ignored in the calculations that have been discussed and still solve for the thick target bremsstrahlung intensities in a reasonable length of time. The Monte Carlo type calculation would be ideally suited for including the above mentioned processes if it were not for its already long computing time. To circumvent this problem, a hybrid calculationcan be made by including the electron transport part of the Monte Carlo calculation in an integration scheme to calculate the bremsstrahlung intensity.

In this scheme, the thick target photon intensity I (k, ϕ) is given by

$$I(k,\phi) = N_A \int_{k+1}^{T_o} \int_0^{2\pi} \int_0^{\pi} e^{-\mu_m t_x/\cos\phi} N_e(E,\epsilon,\psi)\, \sigma_r(E,k,\theta) \sin\epsilon \, d\epsilon \, d\psi \frac{ds}{dE} dE \qquad (2.01)$$

where N_A, T_o, k, u_m, t_x, $\sigma_r(E,k,\theta)$, $\frac{ds}{dE}$, ϕ, ϵ, ψ, and θ have their previously defined meaning and $N_e(E,\epsilon,\psi)$ is the electron distribution function with backscattering included. In evaluating equation (2.01), a Monte Carlo calculation would be used to determine $N_e(E,\epsilon,\psi)$ and t_x. The effects of radiative collisions on the stopping power and the effects of energy straggling on $N_e(E,\epsilon,\psi)$ and t_x can easily be included in the Monte Carlo calculation. The electron transport Monte Carlo calculation takes about five minutes on the IBM 7094 computer to run for 2000 electrons incident on the target. The integral given by equation (2.01), excluding the time taken to evaluate $N_e(E,\epsilon,\psi)$, may be evaluated for nineteen photon angles in 10° steps from 0° to 180° and for twenty equally spaced photon energies in about five minutes of 7094 running time when the Bethe-Heitler formula is used to calculate $\sigma_r(E, k, \theta)$. These points are spaced close enough to allow for the calculation of the photon spectrum integrated over all photon angles. The total time of evaluating equation (2.01) for this number of points is then about ten minutes.

In the following chapters, the form the thin target bremsstrahlung formulas, the electron stopping power formula, the electron distribution function, and the photon attenuation coefficients to be used in equation (2.01) to take in account the elementary processes more accurately will be discussed.

CHAPTER III

THIN TARGET BREMSSTRAHLUNG CROSS SECTION FORMULAS

The quantum mechanical treatment of radiative interactions by Bethe and Heitler form a basis from which the spectral distribution, spatial distribution, and efficiency of the production of X-rays may be calculated for thin targets. A summary of the bremsstrahlung formulas obtained by Bethe and Heitler are presented in a review article by Koch and Motz (ref. 3), and the derivation of the cross section formula and formalism used by these authors will be adopted rather than that of reference 2. The following discussion is taken from reference 3.

The bremsstrahlung cross section $d\sigma$ for the emission of a single photon from a cubic with sides L is given by the transition probability per atom per electron divided by the incoming electron velocity. This cross section can be expressed in dimensions of cm^2 as

$$d\sigma = \frac{2\pi L^3}{(hP_0c/E_0)} \left(\frac{h}{m_0c}\right)^3 \rho_f \left|H_{if}\right|^2 \tag{3.01}$$

where

$$\rho_f = \frac{pE\,h^2 L^6\, dk\, d\Omega_k\, d\Omega_p}{(2\pi)^6 m_0 c^2} \tag{3.02}$$

and E, E_o and P, P_o are the initial and final energy and momentum respectively of the electron, k is the photon energy, $d\Omega p$ and $d\Omega_k$ elements of solid angle in the direction of electron and photon respectively.

The term ρ_f is the density of final states and H_{if} is the matrix element for the transition of the system from an initial state i before the emission of the photon to a final state f after the

emission. $|H_{if}|$ may be written as

$$|H_{if}| = \left(\frac{2\pi e^2}{k\hbar C}\right)(m_0c^2)^2 \left|\int \psi_f^* (\vec{\lambda}^* \cdot \vec{\alpha}) e^{-i\vec{k}\cdot\vec{r}} \psi_i d\tau\right|^2 L^{-9} \qquad (3.03)$$

where $\vec{\lambda}$ is the unit polarization vector of the photon, $\vec{\alpha}$ is the Dirac matrix and ψ_i and ψ_f are the initial and final Dirac wave functions. The cross-section can be written as

$$d\sigma = \frac{137 r_0^2}{(2\pi)^4} \frac{pE_0E}{P_0} \left|\int \psi_f^* (\vec{\lambda}^* \cdot \vec{\alpha}) e^{-i\vec{k}\cdot\vec{r}} \psi_i d\tau\right|^2 k\,dk\,d\Omega_k\,d\Omega_p \qquad (3.04)$$

In order to evaluate the bremsstrahlung cross section formula (3.04) exactly, the matrix element of exact wave functions which describe an electron in a screened nuclear Coulomb field must be used. Unfortunately, it is not possible to solve the Dirac wave equation in closed form because the electron wave function in a coulomb field must be represented as an infinite series (ref. 12). A numerical calculation is possible using exact wave functions, but because of the tediousness of the calculation only a few such calculations have been made to date (ref. 4). Therefore, to evaluate (3.04) it is necessary to use an approximate wave function and, preferably, one that will yield analytical cross section formulas. Since we are in general interested in electrons energies in the relativistic and the near relativistic range, only the Born approximation technique will be discussed. In the Born approximation, the electron is represented by a free particle wave function. Perturbation theory is used to solve the Dirac equation. The cross section formulas obtained by using the Born approximation technique with free particle wave functions, yield relatively simple,

but lengthy, analytical formulas for relativistic energies with or without screening. The Born approximation technique of solving the Bethe-Heitler equations is good provided that

$$\frac{2Zz}{137\beta_0} \ll 1 \tag{3.05}$$

and

$$\frac{2Zz}{137\beta} \ll 1 \tag{3.06}$$

where β_0, β represent the electron velocity divided by the speed of light before and after the radiative collision and Z, z the charge of target atom and electron respectively. Equations (3.05) and (3.06) are always satisfied for electrons of relativistic velocities and light elements except when energy of the emitted photon is nearly equal to the electron energy, the so called high-frequency limit. Even when equations (3.05) and (3.06) are not strictly satisfied, the Born approximation formulas have yielded surprisingly good results.

When equation (3.04) is evaluated for wave functions obtained by the use the Born approximation procedure applied to the Dirac equation, the bremsstrahlung cross section formula, for an unscreened, infinitely heavy nucleus, that is differential with respect to the photon energy k, the photon angle θ_0, and the electrons angles θ and ϕ (see fig. 6) is obtained and is given as

$$[\sigma_r(k,\theta_0,\theta,\varphi)]_{US} = \frac{Z^2}{137}\frac{r_0^2}{4}\frac{dk}{k}\frac{p}{p_0}\frac{d\Omega_k d\Omega_p}{q^4}\left\{\frac{p^2\sin\theta}{(E-p\cos\theta)^2}(4E_0^2-q^2)\right.$$

$$+\frac{p_0^2\sin^2\theta_0}{(E_0-p\cos\theta_0)^2}(4E^2-q^2) - \frac{2pp_0\sin\theta\sin\theta_0\cos\phi(4EE_0-q^2)}{(E-p\cos\theta)(E_0-p_0\cos\theta_0)}$$

$$\left. - \frac{2k^2(p^2\sin^2\theta+p_0^2\sin^2\theta_0-2pp_0\sin\theta\sin\theta_0\cos\phi)}{(E-\cos\theta)(E_0-p_0\cos\theta_0)}\right\} \tag{3.07}$$

where Z = atomic number of target material.

$r_o = e^2 / (m_o c^2) = 2.82 \times 10^{-13}$ cm (classical electron radius).

E_o, E = initial and final total energy of the electron in $m_o c^2$ units.

P_o, P = initial and final total momentum of the electron in $m_o c^2$ units.

k = energy of the emitted photon.

θ_o, θ = angles of p_o and p with respect to k.

ϕ = angle between the planes (p_o, k) and (p, k).

dk = element of solid angle, $\sin\theta d\theta_o d\phi$ in the direction of k.

dp = element of solid angle, $\sin\theta d\theta d\phi$, in the direction of p.

q = momentum transferred to the nucleus in $m_o c^2$ units.

The subscript us denotes the unscreened cross section. The quantities E_o, E, p_o, p, and q may be calculated from the relationships

$$E_o = TT_o + 1 \qquad E = T + 1$$

$$p_o = [T_o(T_o+2)]^{\frac{1}{2}} \qquad p = [T(T+2)]$$

where T_o, T - initial and final energy of the electron in a collision in $m_o c^2$ units.

Equation (3.07) may be corrected for the effects of atomic and nuclear screening by introducing the multiplicative factor $[F_n - F_e]^2$ where F_n and F_e are the nuclear and atomic form factor respectively. The nuclear form factor is roughly equal to one and the atomic form

factor is given by the expression (ref. 13)

$$F_e(q,Z) = \frac{4\pi}{Ze} \int \rho(r)\left(\frac{\sin(qr)}{qr}\right) r^2 dr \qquad (3.08)$$

where $\rho(r)$ is the electron charge distribution, r the radial distance from the center of the atom, and q the momentum transfer to the nucleus. Equation (3.08) has been evaluated by Nelms and Oppenheim (ref. 14) for various elements using the Hartree self-consistent field method and the results are shown in figure 7.

The contribution of the bremsstrahlung resulting from the atomic electrons can also be incorporated into equation (3.07) by a multiplicative factor (ref. 15). If it is assumed that each atomic electron behaves like a simple charged nucleus in the radiation process, equation (3.07) may be made to include the effects of the atomic electrons by multiplying it by $(1 + \frac{1}{Z})$.

The screened differential cross section corrected for the effects of electron-electron bremsstrahlung will then be given as

$$[\sigma_r(k,\theta_0,\theta,\phi)]_s = [1+1/Z][1-F_e(q,Z)]^2[\sigma_r(k,\theta,\theta,\phi)]_{us} \qquad (3.09)$$

To obtain the total cross section for the emission of a photon whose energy is between k and k + dk and the emission angle is between θ_0 and $\theta_0 + d\theta_0$, equation (3.09) must be integrated over all electron angles:

$$[\sigma_r(k,\theta_0)]_s = 2\pi \int_0^{\pi}\int_0^{2\pi} [1+1/Z][1-F_e(q,Z)] \sin\theta_0 [\sigma_r(k,\theta,\theta,\phi)]_{us} d\theta d\phi \qquad (3.10)$$

If screening is neglected, i.e. F_e equal to zero, equation (3.10) may be integrated to give the well-known Beth-Heitler formula for the unscreened cross section differential with respect to photon energy and angle:

$$[\sigma_r(k,\theta_0)]_{US} = \frac{4r_0^2 p}{137(4)kp_0}\sin\theta_0\left\{\frac{8\sin^2\theta_0(2E_0^2+1)}{p_0^2\,\Delta^4} - \frac{2(5E_0^2+2EE_0+3)}{p_0^2\,\Delta^2} - \frac{2(p_0^2-k^2)}{Q^2\,\Delta_0^2}\right.$$

$$+\frac{4E}{p_0^2\Delta_0}+\frac{L}{pp_0}\left[\frac{4e\,\sin^2\theta_0(3k-p_0^2E)}{p_0^2\,\Delta_0}+\frac{4E_0^2(E_0^2+E^2)}{p_0^2\,\Delta^4}+\frac{2-2(7E_0^2-3EE_0+E^2)}{p_0^2\,\Delta_0^2}\right.$$

$$\left.\left.\frac{2k(E_0^2+EE_0-1)}{p_0^2\,\Delta_0}\right]-\left[\frac{4\epsilon}{p\Delta_0}\right]+\left[\frac{\epsilon^Q}{pQ}\right]\left[\frac{4}{\Delta_0^2}-\frac{6k}{\Delta_0}-\frac{2k(p_0^2-k^2)}{Q^2\Delta_0}\right]\right\} \tag{3.11}$$

where

$$L = \ln\left(\frac{EE_0 - 1 + pp_0}{EE_0 - 1 - pp_0}\right)$$

$$\Delta_0 = E - p_0\cos\theta_0$$

$$\epsilon = \ln\left(\frac{E+p}{E-p}\right)$$

$$\epsilon^Q = \ln\left(\frac{Q+p}{Q-p}\right)$$

$$Q^2 = p_0^{\,2} + k^2 - 2\,p_0 k\cos\theta_0$$

A comparison of the unscreened and the screened bremsstrahlung cross sections, is made in figures 8a, 8b, and 8c for a number of photon energies and angles. In these figures, the ratio of the unscreened cross section to the screened cross section is shown at various photon energies for aluminum, iron, and gold at electron energies of .5, 1.0, and 2.0 MeV. The screened cross sections $\left(\frac{d\sigma}{dkd\theta}\right)_s$ were computed by numerically integrating equation (3.10), and the form factor values were determined from the curves shown in figure 7 (ref. 14). The comparison show, as is to be expected, that the screened cross sections differ significantly from the unscreened cross sections only for small photon emission angles and low photon energies and that the difference increases with increasing atomic number.

At the high frequency limit, i.e. that point where the photon energy is equal to the electron energy, the Born approximation is grossly violated, and the Bethe-Heitler formula predicts a zero cross section. This shortcoming of the Bethe-Heitler formula has been emphasized by various experimental studies (ref. 16 and 17) which indicate that the cross section has a finite value at the high frequency limit.

A Sauter approximation method has been used by Fano (ref. 18) to evaluate the bremsstrahlung cross section at the high frequency limit. In this calculation, which applies to an outgoing electron with velocity near zero, the bremsstrahlung cross section is related to the photoelectric cross section by detail-balance arguments and involves expansions in power of $Z/137\beta_o$ and $Z/137$ instead of $Z/137\beta$ as used in

the Born approximation (β_0 and β are, respectively, the incoming and outgoing electron velocities divided by the speed of light). The cross section formula differential in photon energy and angle for the high-frequency limit as obtained by Fano is given as

$$[\sigma_r(k,\theta)]_{k=T_0} = \frac{Z^3 r_0}{137}\frac{dk}{k}\frac{\beta_0}{k^2 E_0^3}\frac{4\pi \sin\theta d\theta}{(1-\beta_0\cos\theta)}[1+.5E_0(E_0-1)(E_0-2)(1-\beta_0\cos\theta)] \qquad (3.12)$$

This formula when integrated over θ gives

$$[\sigma_r(k)]_{k=T_0} = \frac{4\pi Z^3 r_0}{137}\frac{dk}{k}\frac{E_0\beta_0}{(E_0-1)^2}\left\{\frac{4}{3}+\frac{E_0(E_0-2)}{E_0-1}\left[1-\frac{1}{2\beta E_0^2}\ln\left(\frac{1+\beta_0}{1-\beta_0}\right)\right]\right. \qquad (3.13)$$

A comparison is shown of the cross section values predicted by equation (3.12) and the experimentally measured values for aluminum for electron energies of .05, .5, and 1.0 MeV (ref. 18) in figure 9. The comparison shows that the theoretical cross sections are within experimental limits of the measured values for aluminum at these energies.

In figures 10a and 10b, the screened and unscreened cross sections as predicted by equations (3.09) and (3.10) as well as the cross section at the high frequency limit is compared with the experimental data (ref. 19) for aluminum at photon emission angles of 15° and 30° and electron energies of .5 and 1.0 MeV. The screened cross sections were computed by numerically evaluating the integral given by equation (3.09) and making use of the form factor values given in figure 7. From these figures, it is seen that the screened cross section is lower than the unscreened cross section at low photon energies and more closely approximates the measured values. At the

intermediate photon energies, the screened and unscreened cross sections are equal and at the high energy photon region both cross sections underestimate the measured cross section values. The theoretical cross section at the high frequency limit is above the Bethe-Heitler cross section and is very near the measured values. At these electron energies and photon angles for aluminum, it appears that the experimentally measured value can be approximated quite well by using the screened cross section formula (equation 3.09) for low energy photon, the unscreened cross section formula for intermediate photon energies (equation 3.11), and the formula due to Fano equation (3.12) for the cross section at the high frequency limit.

CHAPTER IV

STOPPING OF ELECTRONS BY MATTER

Energy is lost by electrons as they pass through matter primarily by inelastic collisions with the atomic electrons and radiative interactions with the atomic nuclei. The importance of each of these processes is dependent on the energy of the electron and the atomic number of the stopping material. The point at which the mean value of the ionization and radiative loss are equal is called the critical energy. A graph of the critical energy as a function of the atomic number as calculated from the empirical expression given by Berger (ref. 19) as

$$T_{crit} = \frac{800}{Z+1.2} \quad \text{MeV} \tag{4.01}$$

is shown in figure 11. The circles on the graph are values calculated by Berger from theoretical considerations. The critical energy varies from 403 MeV for the hydrogen molecule to 8.36 MeV for uranium, and gives a convenient dividing point for determining when which of the energy loss mechanism is the most important.

A very detailed calculation of the energy loss and range of electrons in matter which considers both ionization and radiative losses has recently been made by Berger and Seltzer (ref. 19) and the following discussion borrows liberally from this work.

The total stopping power for electrons is given as the sum of the mean ionization and radiative energy losses per unit path length in gm/cm^2 as

$$-\frac{1}{\rho}\left(\frac{dE}{ds}\right)_{Tot} = -\frac{1}{\rho}\left(\frac{dE}{ds}\right)_{ion} - \frac{1}{\rho}\left(\frac{dE}{ds}\right)_{rad} \tag{4.02}$$

where ρ is the density of the stopping media.

The mean ionization loss may be calculated from the Bethe stopping power theory, and using the formulation of Rohrlich and Carlson (ref. 20) is given by

$$-\frac{1}{\rho}\left(\frac{dE}{ds}\right)_{ion} = \frac{2\pi N_A r_0 m_0 c^2}{\beta^2}\,\frac{Z}{A}\left\{\log\left[\frac{\tau(\tau+2)}{2(I/m_0c^2)^2}\right] + F(\tau) - \delta\right\} \qquad (4.03)$$

where m_0c^2 is the electron rest mass energy, τ is the electron kinetic energy in m_0c^2 units, $\beta = [\tau/\tau + 2]^{\frac{1}{2}} / (\tau + 1)$, Z and A the atomic number and weight respectively of the stopping medium, I the mean ionization energy, N Avogadro's number, Π_0 the classical radius of the electron, and δ the density effect correction. The mean ionization energy I can, in principal, be calculated theoretically; however, because of a scarcity of detailed data necessary for the calculation, I is usually determined empirically through analysis of data from stopping power experiments. Experimental data for protons or other heavy charged particles are usually used, rather than electron data, because the energy loss straggling and multiple scattering corrections are easier to make. Mean ionization energies obtained in this manner, are subject to considerable uncertainties; however, since I enters equation (4.03) logarithmically, the error it introduces in the stopping power is considerably less than the error in itself. Various empirical formulas have been proposed to relate I and the atomic number, and we will adopt the one used in reference 11 for $Z \geq 13$

$$I = Z\,(9.76 + 58.8/Z^{1.19})\ \text{eV} \qquad (4.04)$$

The reduction of the ionization loss due to polarization of the medium is taken in account by the density effect correction, δ . Berger, et al, have calculated the percent reduction in the ionization energy loss due to the density effect for several materials for electron energies from .1 to 1000 MeV using the empirical formulas of Sternheimer (ref. 21) and a list of the values they obtained are shown in Table I. Since the density effect corrections are not too large for relatively low electron energies, an interpolation between values given in Table I may be used to make this correction to the ionization losses rather than the empirical formulas of Sternheimer.

The Bethe-Heitler theory may be used to calculate mean radiative energy loss. The energy loss per gm/cm^2 is given as

$$-\frac{1}{\rho}\left(\frac{dE}{ds}\right)_{rad} = -\frac{N_A}{A}\int_{E_0}^{0}\int_{k+1}^{E_0}\int_{0}^{2\pi} k[\sigma_r(k,\theta_0)]_s \, d\theta_0 dk dE \qquad (4.05)$$

where N_A is Avogodro number, A the atomic number of the target matter, k the photon energy, and $[\sigma_r(k,\theta_o)]_s$ the screened thin target cross section given by equation (3.10). The mean radiative energy loss predicted by this formula will be somewhat lower than the value calculated by Berger, et al, for electron energies below 15 MeV since he did not include screening in this energy range.

The mean ionization loss, the mean radiative loss, and the total stopping power for aluminum, iron, and gold for electrons in the energy range between .01 MeV and 1000 MeV are shown in figures 12a, 12b, and 12c (the values above 15 MeV are taken from ref. 19). The mean radiative loss is seen to be relatively unimportant for aluminum

and iron for electron energies below about 10 MeV. For gold, however, the mean radiative and ionization loss become equal at about 8 MeV.

The mean range of the electron is determined by integrating equation (4.02):

$$s = \int_{T_0}^{0} \frac{1}{\rho} \left(\frac{dE}{ds}\right)_{Tot} dE \qquad (4.06)$$

The range of electrons in aluminum, iron, and gold obtained from equation (4.06) for electrons energies from .01 MeV to 1000 MeV is shown in figure 13. The mean electron range increases fairly linearly with energy initially and then flattens out at the higher electron energy because the radiative energy loss becomes large.

The discussion thus far has dealt with only mean energy loss. However, since electrons are very light, a considerable fluctuation in the energy loss by the electron in passing through even a very thin target occurs. The problem of energy fluctuation has been treated theoretically by Landau (ref. 22) for ionization losses for the case when the energy lost by the electron in passing through the target is small compared to the energy of the particle. The distribution function W_I that describes the fluctuation in energy loss ΔE obtained by Landau may be expressed as

$$W_I(\Delta E)d(\Delta E) = W_L(\lambda)\, d\lambda \qquad (4.07)$$

where $$\lambda = \frac{\Delta E - \overline{\Delta E}}{N_A Z c s} \qquad (4.08)$$

$$c = \frac{2\pi e^4}{m v^2} \qquad (4.09)$$

and where $\overline{\Delta E}$ is the average energy loss, s the distance traversed by the electron in losing ΔE, N_A the number of atoms/cm^3 and Z, m, and v have their usual meaning. $W_L(\lambda)$ is a universal function that has been tabulated by Börsch-Supan (ref. 23) and a graph of which is shown in figure 14.

The energy loss distribution is asymmetric and is characterized by broad peaking about the most probably energy loss (which is significantly less than the mean energy loss) and a high energy loss tail. This curve may be used to determine the fluctuation in energy lost by an electron in traversing a distance s.

CHAPTER V

ANGULAR AND ENERGY DISTRIBUTION OF ELECTRONS IN A THICK TARGET

The penetration of electrons through matter is characterized by multiple scattering in the coulomb field of the atoms of the stopping medium and statistical fluctuation in the rate of energy loss. For thin targets, the scattering and energy straggling have been treated analytically with results that agree satisfactorily with experiment. For targets whose thickness is such that the electron mean scattering angle is comparable to a radian, analytical expressions for the electron angular distribution in terms of the electron penetration are non-existant except for the most idealized case (ref. 24). The thick target case is amenable to a Monte Carlo calculation and such calculations have been made by Berger and a number of investigators (ref. 25, 26, and 27). A detailed outline of the Monte Carlo method as applied to electron penetration has been given by Berger, (ref. 27) and much of the following discussion is derived from his article.

Because the number of collisions undergone by a fast electron in slowing down is so large, it is not feasible to simulate individual collisions. For example, Berger (ref. 27) calculated that 10^5 elastic collisions occur during the stopping of a .5 MeV electron in aluminum. To circumvent this problem, the path of the electron is subdivided into a relatively small number of short segments in which the mean scattering angle is relatively small so that the analytical treatment gives a

satisfactory approximation to the probability distribution of the net angular deflection. The problem may then be treated as if the electron suffered a single elastic collision at the end of each segment.

To determine analytically the electron angular distribution at the end of each segment, the multiple scattering theory of Goudsmit and Saunderson may be utilized (ref. 28). From this theory, the angular distribution of initially monodirectional and monoenergetic electrons whose kinetic energy has been reduced from T_o to E in a continuous manner may be calculated from the expression

$$N(E,\epsilon) = \sum_{\ell=0}^{\infty} (\ell + \tfrac{1}{2}) \exp\left[-\int_{E_0}^{E} G_\ell(E')\right] P_\ell(\cos\epsilon)\, dE' \qquad (5.01)$$

$$G_\ell(E') = 2\pi N_A(E') \int_0^{\pi} \sigma(E',\theta)[1 - P_\ell(\cos\theta)]\sin\theta\, d\theta \qquad (5.02)$$

where $N(E, \epsilon)$ is the probability that an electron of energy E will be traveling at an angle of ϵ with respect to its initial direction, $P_\ell(\cos\epsilon)$ and $P_\ell(\cos\theta)$ are Legendre polynomials, $N_A(E')$ is the number of target atoms in the energy interval between E' and $E' + dE$, and $\sigma(\theta, E')$ the electron single scattering cross section. The quantity $N_A(E')$ can be calculated from the stopping power formula equation (4.03) and the screened relativistic single-scattering cross section may be obtained from the following expression:

$$\sigma(E,\theta) = \frac{\sigma_M(E,\theta)}{\sigma_R(E,\theta)} [\sigma_R(E,\theta)]_s$$

where $[\sigma_R(E, \theta)]_s$ is the screened Rutherford cross section at polar angle θ for an atom of atomic number Z, and $\sigma_M(E, \theta) / \sigma_R(E, \theta)$ is the ratio of the unscreened Mott cross section to the unscreened

Rutherford cross section. The values of the somewhat awkward to calculate ratios of Mott to Rutherford cross section have been tabulated in some detail by Doggett and Spencer (ref. 29).

The screened Rutherford cross section values may be calculated from the formula (ref. 27)

$$[\sigma_R(E,\theta)]_s = \frac{Ze^4}{p^2v^2(1-\cos\theta + 2\eta)^2} \qquad (5.04)$$

where Z, e, p, and v have their usual meaning and η, the Moliere screening parameter (ref. 27), is given for electrons by the expression

$$\eta = 1.7 \times 10^{-5} Z^{2/3} \left[1.13 + 3.76 \frac{Z}{137\beta}\right] \qquad (5.05)$$

A phenomenological description of the manner in which the Monte Carlo method was applied to determine the electron distribution $N(E, \epsilon, \psi)$ in a thick target for use in equation (2.01) is as follows. The direction of the electron incident on the target was taken to be normal and allowed to penetrate a distance s_1 into the target. At the distance s_1, the direction of the electron is allowed to change by permitting the polar angle, θ, to change anywhere from 0° to 180° with a probability consistent with the distribution function given by equation (5.01) and permitting the azimuthal angle, ϕ, to also change anywhere from 0° to 180°, but with an equal probability since the medium is considered to be isotropic and polarization is disregarded. The energy lost by the electron in the distance s_1 is also a variable, the value being determined from the Landau distribution function given by equation (4.07). At this point, the energy and direction of the

electron is recorded as well as its perpendicular distance of penetration as calculated from the equation

$$x_1 = s_1 (\cos\theta_0 \cos\theta_1 + \sin\theta_0 \sin\theta_1 \cos\phi) + s_0 \qquad (5.06)$$

This procedure is now repeated, only the electron's energy and direction is different, and this procedure is continued until the electron has lost all of its energy or is backscattered out of the target. The complete procedure of keeping track of the electron's energy, direction, and position in the target is repeated for n electrons. The angular distribution of electrons in the target as a function of the electron's energy is determined by adding up the number of electrons whose energy is between E and $E + \Delta E$ that are traveling in the direction between θ and $\theta + \Delta\theta$. The average distance of penetration $\bar{x}(E)$ is determined from the formula

$$\bar{x}(E) = \left[\sum_i x_i(E)\right] / \left[\sum_i n_i(E)\right] \qquad (5.07)$$

where $x_i(E)$ the distance traveled by the ith electron when its energy has been reduced from T_o to E and $n_i(E)$ is the number of electrons in the target of energy E.

The accuracy of the results calculated using this method can not be determined directly since it is not possible to measure the angular and energy distribution of electrons inside the target. However, it is possible to use the Monte Carlo method as outlined to calculate the angular and energy distribution of electrons transmitted through foils of various thickness, and these results may be compared with experimental results to gauge the accuracy of the Monte Carlo technique employed. Also, backscattering of electrons from a target

may be used as a check on the accuracy of the technique.

In figure 15a, 15b, and 15c, a comparison of the results obtained by use of the method described above and experimental data (ref. 30) for the transmission of 1 MeV electrons through foils .11, .22, and .33 grams/cm^2 thick. These thicknesses represent 20%, 40%, and 60% of the mean range of a 1 MeV electron in aluminum. In the calculation the target was divided into 40 segments, each corresponding to a loss of 25 KeV and a total of 10,000 particles were traced. The curves indicate that reasonably correct results can be expected from this method of calculation, especially for the case when the electron's energy has not been reduced by a substantial amount. After the electrons have traveled a perpendicular distance equal to about 60% of their range, deviation from the theoretical values are observed. A comparison with transmission data for gold (not shown) indicate the same general trend as that for aluminum.

A comparison of the fractional number of backscattered electrons calculated from the Monte Carlo program and experimental data (ref. 31) is made in figure 16. The comparisons indicate good agreement between theory and experiment for the fractional number of backscattered electrons for all Z numbers.

From the comparisons made, it is expected that the Monte Carlo method employed will predict reasonably accurate results for the angular and energy distribution and perpendicular distance of penetration for electrons with the same order of energy as those compared for all Z number materials. The accuracy will be best when the

electron's energy is not too severely degraded. At low electron energies, deviations are expected. The inaccuracy at the lower electrons energies, however, will not have a large effect on the calculation of the thick target bremsstrahlung spectra since most of the bremsstrahlung is produced at the higher electron energies.

CHAPTER VI

PHOTON ATTENUATION IN A TARGET

High-energy photons passing through matter are attenuated primarily by three distinct elementary processes. These processes are the photoelectric effect, Compton scattering, and pair production.

In the photoelectric effect, the photon disappears and its energy is transferred to an atomic electron, usually one from the inner shell. This effect predominates for low energy photons. The photoelectric cross section decreases rapidly with increasing gamma energy and increases with the atomic number of the target material.

A photon is scattered inelastically in Compton scattering with part of its energy transferred to an atomic electron. The direction of the photon is also changed. This effect predominates over a large energy range in low Z materials and from about 1-5 MeV in high Z materials.

The photon energy must be greater than $2\ m_o c^2$ (where $m_o c^2$ is the rest mass energy of the electron and is equal to .511 MeV) for pair production to occur. In this process, the photon disappears and its energy is transferred to an electron-positron pair. This effect predominates for high-energy photons, especially in materials with high Z numbers.

The probability $P(Z,t)$ that a photon of energy E will traverse a target of atomic number Z and thickness t without its energy or

direction changed is given by the exponential formula

$$P(Z,t) = \exp(-u(Z,E)t) \qquad (6.01)$$

where μ (Z,E) is the mass attenuation coefficient. The mass attenuation coefficient is the sum of the attenuation coefficients for the three processes discussed above and is a function of the photon energy and Z number of the target material.

The mass attenuation coefficients are obtained experimentally and have been tabulated for a wide range of materials and photon energies by Davisson (ref. 32). The mass attenuation coefficients used in evaluating equation (2.01) were obtained by a linear interpolition between the values given in Table II that is taken from reference 32.

The secondary radiation produced by the photon interaction in the target material can be significant for very thick targets and must be taken into account by the so called buildup factors (ref. 33). However, for target thicknesses that are to be considered in this thesis, the secondary radiation is of little consequence.

CHAPTER VII

EVALUATION OF THE THICK TARGET BREMSSTRAHLUNG INTEGRAL

Now that the functional form of the thin target bremsstrahlung cross section formulas, the electron distribution function, the stopping power formula, and the attenuation formula has been discussed, the problem of calculating the thick target bremsstrahlung intensity, $I(k, \varphi)$, has been reduced to the problem of evaluating the integral given by equation (2.01), which is repeated below for reference:

$$I(k,\phi) = N_A \int_{k+1}^{T_o} \int_0^{2\pi} \int_0^{\pi} e^{-\mu_m \rho x/\cos\phi} N_e(E,\epsilon,\psi)\, \sigma_r(E,k,\Theta) \sin\epsilon \, d\epsilon \, d\psi \frac{ds}{dE} \, dE \qquad (2.01)$$

To obtain values for $I(k, \phi)$ the above integral was numerically evaluated since an exact integration to obtain an analytic formula for $I(k, \phi)$ is not possible. In the numerical evaluation of the integral, a Simpson rule integration was made, and the various forms of the functions discussed in Chapters 3 through 6 were used to calculate the integrand. An IBM 7094 computer was used to make the numerical integration.

The form of the thin target bremsstrahlung formula used depended on the energy of the electron and the emitted photon as well as the photon emission angle. At photon energies and angles where screening was important, a numerical integration of equation (3.09) was made to determine the cross section values. When the photon's energy and

angles were such that the value of the screened and unscreened cross section were equal to within 1%, equation (3.10) was used from this point until the photon energy was equal to 90% of its maximum value. The bremsstrahlung cross section for photons whose energy laid between 90% of its maximum value and its maximum value was calculated by interpolating between the cross section value given by equation (3.10) and the cross section predicted by the high frequency limit formula given by equation (3.12).

Numerical values for the electron distribution, $N_e(E, \epsilon, \psi)$, as a function of the electron energy and direction were obtained from a Monte Carlo type calculation described in Chapter V. In this calculation the Goudsmit-Saunderson multiple scattering theory was evaluated for a screened, relativistic, single-scattering cross section section; the stopping power computed from equation (4.02); and the Landau distribution function was used to include the fluctuation in energy loss. The average distance of perpendicular penetration $x_i(E)$ as a function of energy was also obtained from the Monte Carlo calculation.

The photon attenuation coefficients were taken from experimental data, the values of which are given in Table II (ref. 32).

The interval of integration used for the angle variables ϵ and ψ was 10°, and the interval for the energy variable E depended on the photon energy. An energy interval, ΔE, equal to To/20 was used for $k > \frac{1}{2}$ to, and for $k < \frac{1}{2}$ to, $E = T_o/40$. The accuracy of the integration

for these intervals was checked by cutting the intervals in half. In all cases checked, the values obtained from the use of the full and one half increments in evaluating equation (2.01) agreed within 2%.

The values for the photon intensity, I(k), were obtained by integrating $I(k, \phi)$ over the angle variable. The interval of integration used for ϕ was 10°. A check on the accuracy of this integration was also made by cutting the interval in half.

CHAPTER VIII

COMPARISON OF THEORETICAL PHOTON INTENSITY WITH EXPERIMENTAL DATA

Recently a fairly substantial amount of experimental thick target bremsstrahlung data for a wide range of electron energies and target materials has become available. Experimental data for the photon intensity differential in photon energy and angle and photon intensity differential in energy, for .5 to 3.0 MeV electrons incident on thick aluminum and iron targets and for 1.0 and 2.8 MeV electrons incident on thick gold targets have been measured by Dance, et al (ref. 9). This data will be used for comparison of the theoretically calculated photon intensities.

The theoretical photon intensities, differential in photon energy and angle, resulting from electrons of energy .5, 1.0, 2.0 and 3.0 MeV striking thick aluminum targets are compared with the experimental data in figures 17, 18, 19, and 20. The theoretical photon spectrum was calculated by numerically evaluating equation (2.01), and the values that are plotted are k times $I(k, \phi)$, in units of MeV/MeV-sr-electron. Similar comparisons are made for thick iron and gold targets in figures 21, 22, 23, 24, and 25. The experimental data is estimated by Dance, et al to be accurate to ± 20% in absolute value.

The theoretical intensities for bremsstrahlung produced in thick aluminum targets by .5 and 1.0 MeV electrons (figures 17 and 18) agree with experimentally measured intensities within the experimental error (± 20%) except at the very high photon energies. At these

photon energies, the theoretical intensity underestimates the measured intensity in some cases by 50%. The theoretical intensities for bremsstrahlung produced in thick iron targets by .5 and 1.0 MeV electrons (figures 21 and 22) agree with the measured value within experimental error for the low photon energies and angles, however, the theoretical intensities underestimate the measured values at the high photon energies. The theoretical electron-bremsstrahlung intensities for 2.0 and 3.0 MeV electrons incident on aluminum and iron targets (figures 19, 20, 23, and 24) agree within experimental error with the measured values at all photon energies and angles except at 0°. At this angle the theoretical value overestimates the measured value by roughly a factor of two. The calculated intensity for 1.0 MeV electrons incident on a thick gold target (figure 25) underestimates the measured intensity at photon energies greater than 300 keV.

In figures 26 and 27, comparisons are made of the theoretical and experimental photon intensities integrated over all photon angles for electron-bremsstrahlung produced by .5, 1.0, 2.0, and 3.0 MeV electrons in thick aluminum and iron targets. Excellent agreement is found for all electron energies and photon energies for these targets. The agreement between the calculated and measured values for the photon intensity, differential in photon energy, produced by 2.8 MeV electrons stopped in gold (figure 28) is not as good as that obtained for the aluminum and iron targets. The calculated intensity underestimates the measured intensity at the high photon energies by a factor of about two.

Comparisons of the theoretical photon intensity calculated from equation (2.01) and that calculated by Scott (ref. 8) with experimental data are made in figures 29 and 30. As can be seen from these figures, the comparison indicates that better agreement with experiment is to be had by using equation (2.01) rather than equation (1.05) that is due to Scott.

CHAPTER IX

CONCLUDING REMARKS

The theoretical values predicted by the computational model adopted in this thesis are in reasonably good agreement with experimentally measured values for bremsstrahlung produced by electrons with energies from .5 to 3.0 MeV that are stopped in aluminum and iron and for 1.0 and 2.8 MeV electrons stopped in gold. The extent of the agreement of the calculated and measured thick target bremsstrahlung intensities obtained is better than obtained in early work (ref. 4 and 6) especially at the low and high photon energies. The closer agreement results primarily from using a combination of thin target bremsstrahlung formulas; namely, the screened Bethe-Heitler formula for low photon energies, the unscreened Bethe-Heitler formula for intermediate photon energies, and the Sauter-Fano formula at the high-frequency limit, instead of just the unscreened Bethe-Heitler formula for all photon energies as was done in earlier work. More exacting calculations of the electron distribution in the target and the attenuation of the photons by the target also contribute to the closer agreement obtained.

At this point the question must be asked, "Why is good agreement obtained between the calculated and measured values for thick target bremsstrahlung when the approximation (Born approximation) used in deriving the thin target bremsstrahlung formula is grossly violated for the low electron energies?" The answer to this question lies in the following facts: (1) the Bethe-Heitler formula, even when the

Born approximation is violated, seems to predict thin target cross sections that agree fairly closely with the measured values (see ref. 3, p. 922); (2) the majority of the bremsstrahlung is produced at the front of the target when the electron's energy is still fairly high, and therefore the inaccuracies of the Bethe-Heitler formula when the electron's energy has been degraded to a low value are not strongly reflected by the thick target results.

The fact that most of the bremsstrahlung is produced in the front of the target also helps to obscure the inaccuracies of the electron multiply scattering theory that occur after the electron energy has been degraded to a fraction of its initial value.

It is expected that the computational model adopted here can be used to calculate thick target bremsstrahlung intensities for higher electron energies than 3 MeV for low Z number material. The energy region of applicability of the calculated model is limited by the multiple scattering formula because it is based only on coulomb scattering and does not take in account scattering of the electron due to radiative collisions. The upper limit on the electron energy should be no greater than one-half of the critical energy (see figure 11) in order that scattering due to radiative collisions can be neglected. This condition imposes an upper limit of $\approx$ 25 MeV and $\approx$ 4.5 MeV for aluminum and gold respectively. The lower limit for the electron energy is governed primarily by the accuracy of the bremsstrahlung cross section formulas. Since it is not known at what energy the cross section formulas give unreliable results, it is difficult to give an absolute value for this energy.

REFERENCES

1. A. Sommerfield, Wellenmechanik (Frederick Vngar, New York, 1950) Chapter 7.
2. H. Bethe and W. Heitler, Proc. Roy. Soc. (London) A146, 83 (1934).
3. H. W. Koch and J. W. Motz, Rev. Mod. Phys. 31, 920 (1959).
4. C. D. Zerby, NASA Contractor Report.
5. W. C. Miller, J. W. Motz, and C. Cialello, Phys. Rev. 96, 1344 (1954).
6. R. Wilson, Proc. Phys. Soc. 66A, 638 (1953).
7. H. A. Kramers, Phil. Mag. 46, 836 (1923).
8. W. W. Scott, A Formula for Predicting the Angular Distribution of Thick Target Bremsstrahlung, a thesis presented the College of William and Mary, 1965.
9. W. E. Dance, L. L. Baggerly, J. H. Johnson, and H. B. Gibbons, LTV Contract Report Number 0-71000/5R-13, May 1965.
10. W. W. Scott, NASA TND-2659.
11. M. J. Berger and S. M. Seltzer, Paper presented at Second Symposium on Protection Against Radiation Hazards in Space, Gatlinburg, Tennessee, October 12-14, 1964.
12. L. C. Maximon, Phys. Rev. 93, 768 (1954).
13. H. Bethe and W. Heitler, Quantum Theory of Radiation (Oxford University Press, London, 1954).
14. A. T. Nelms and I. Oppenheim, J. Research Natl. Bur. Standards 55, 53 (1953).
15. B. Rossi, High Energy Particles (Prentice-Hall, New York, 1952).

16. W. C. Miller and B. Waldman, Phys. Rev. 75, 425 (1949).

17. W. C. Miller and B. Waldman, Phys. Rev. 109, 630 (1958).

18. U. Fano, H. W. Koch and J. W. Motts, Phys. Rev. 112, 1679 (1958).

19. M. J. Berger and S. M. Seltzer, Tables of Energy Losses and Ranges of Electrons and Positrons, NASA SP-3012, 1964.

20. F. Rohrlick and B. C. Carlson, Phys. Rev. 93, 38 (1954).

21. R. M. Sternheimer, Phys. Rev. 88, 851 (1952); 91, 256 (1953); 103, 511 (1956).

22. L. Landua, J. Physics, USSR 8, 201 (1944).

23. W. Börsch-Supan, J. Research Natl. Bur. Standards 65B, 245 (1961).

24. R. D. Birkhoff, in Handbuch der Physik (S. Flugge, ed.), vol. 34, p. 53 (1958). Springer, Berlin.

25. J. E. Leiss, S. Penner, and C. S. Robinson, Phys. Rev. 107, 1544 (1957).

26. J. F. Perkins, Phys. Rev. 126, 1781, (1962).

27. M. J. Berger, In Methods of Computational Physics, Vol. 1, p. 135 (1961). Academic Press, New York.

28. S. Goudsmit and J. L. Saunderson, Phys. Rev. 57, 24 (1940).

29. J. A. Doggett and L. V. Spencer, Phys. Rev. 103, 1597 (1956).

30. W. E. Dance and W. J. Rainwater, NASA Publication CR-334, December 1965.

31. K. A. Wright and J. G. Trump, Phys. Rev. 33, 687 (1962).

32. C. M. Davisson, In Beta - and Gamma-Ray Spectroscopy, (K. Seigbahn, ed.), p. 827 (1965). North Holland, Amsterdam.

33. V. Fano, Nucleonics, Vol. 9, No. 9, Sept. 1953.

34. W. E. Dance, private communication.

VITA

Chris Gross

Born in Charlotte, North Carolina, September 17, 1937. Graduated from New Hanover High School in Wilmington, North Carolina, June 1955; Bachelor of Science in Nuclear Engineering, North Carolina State University, January 1962.

In September 1963, the author entered the College of William and Mary as a graduate student in the Department of Physics under the NASA graduate study program.

TABLE 1[†]

Percent reduction of collision energy loss
due to density effect

T (MeV)	H_2*	C	Al	Cu	Ag	Au
0.1	0.0	0.0	0.0	0.0	0.0	0.0
0.2	0.0	0.4	0.0	0.0	0.0	0.0
0.5	0.0	1.2	0.5	0.5	0.1	0.0
1.0	0.0	2.7	1.5	1.5	0.7	0.7
2.0	0.0	4.8	3.4	3.4	2.2	2.0
5.0	0.0	8.5	6.8	6.8	5.3	4.9
10	0.0	11.8	9.8	9.9	8.2	7.6
20	0.0	15.2	13.1	13.3	11.3	10.7
50	0.7	19.5	17.3	17.6	15.7	14.9
100	3.3	22.5	20.3	20.7	18.8	18.1
200	6.6	25.1	23.1	23.6	21.8	21.1
500	10.6	28.1	26.4	27.0	25.4	24.8
1000	13.4	30.1	28.6	29.2	27.8	27.3

* Normal pressure.

† From reference 19.

TABLE 2

Mass Absorption Coefficients (cm^2/gm)*

MATERIALS			
Photon Energy (MeV)	Aluminum	Iron	Lead
.01	25.8	179.	137.
.02	3.22	25.0	90.
.03	1.03	7.91	30.6
.04	.492	3.46	14.3
.05	.319	1.80	7.96
.06	.246	1.11	4.72
.08	.185	.550	2.12
.1	.160	.342	5.56
.2	.120	.139	.937
.3	.103	.106	.370
.4	.0922	.0921	.219
.6	.0778	.0763	.118
.8	.0684	.0665	.0851
1.0	.0614	.0596	.0684
2.0	.0432	.0425	.0451
3.0	.0353	.0361	.0417
4.0	.0310	.0331	.0415
5.0	.0283	.0314	.0423
6.0	.0265	.0305	.0433
8.0	.0242	.0297	.0458
10.0	.0230	.0296	.0487

*From reference (32).

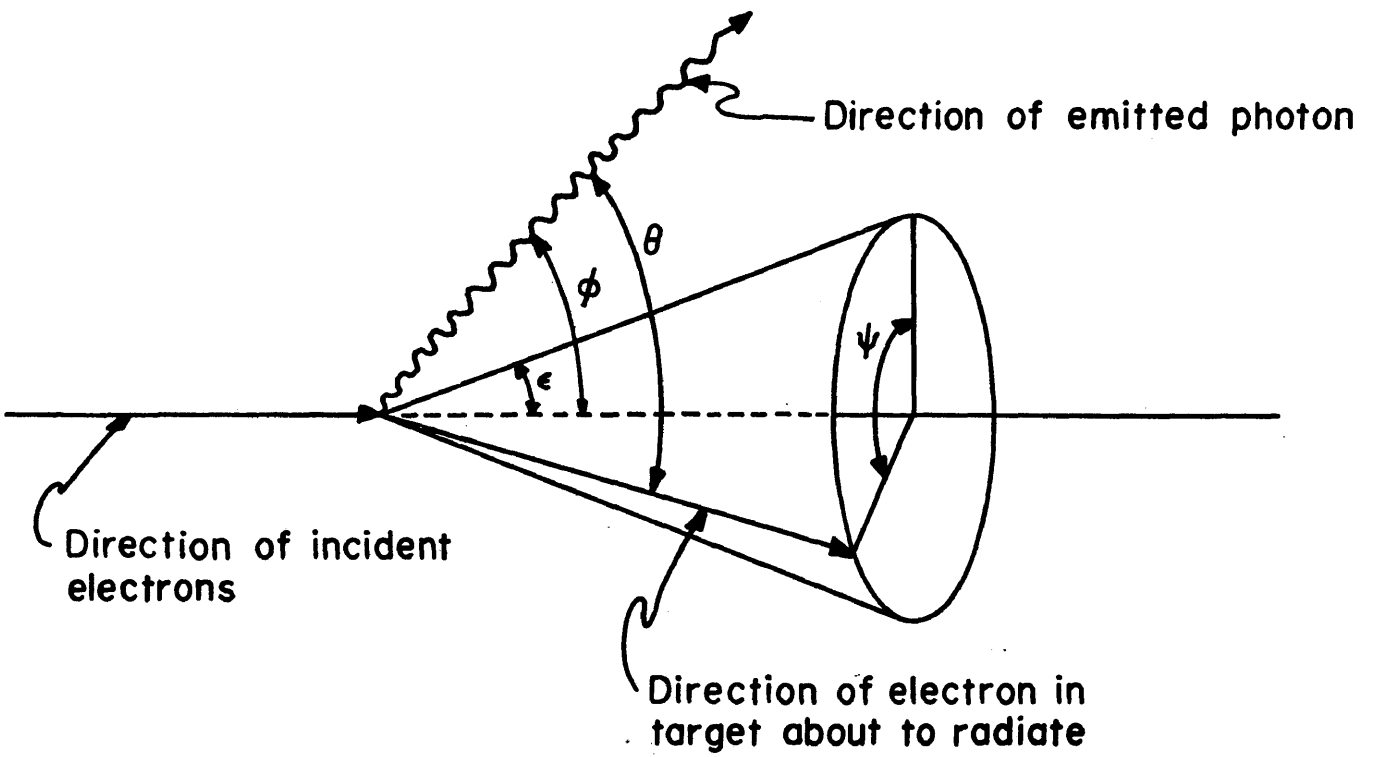

Figure 1. - Collision geometry for thick target bremsstrahlung.

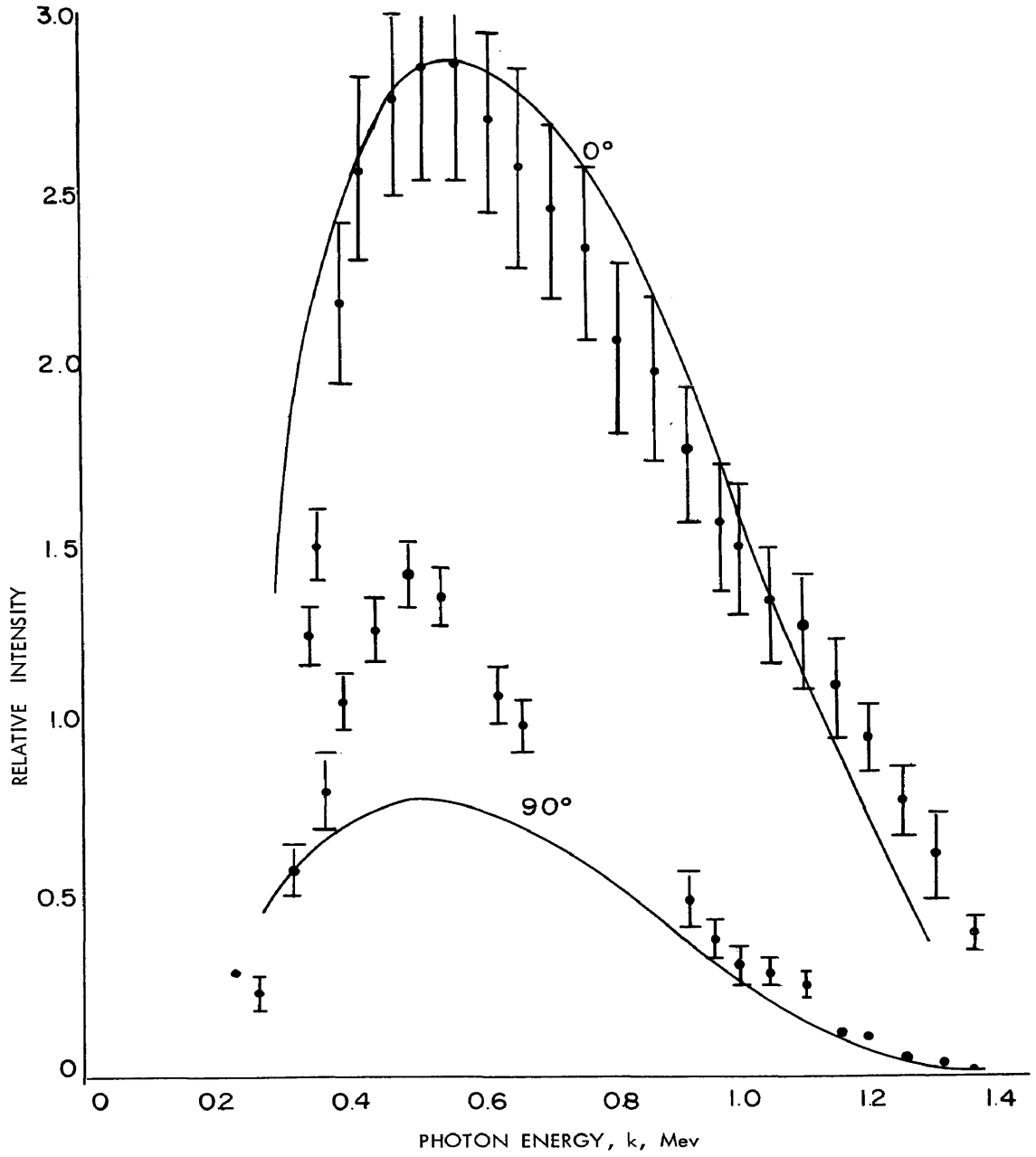

Figure 2. - Comparison of theoretical and experimentally determined relative spectral intensities obtained by Miller et al (ref. 8) at photon angles of 0° and 90° for 1.4 MeV electrons incident on a thick tungsten target. To obtain absolute spectral intensities, in MeV per steradian per MeV per incident electron, the ordinate should be multiplied by 10^{-3} for the computed curves, and by 2.1×10^{-3} for the experimental points.

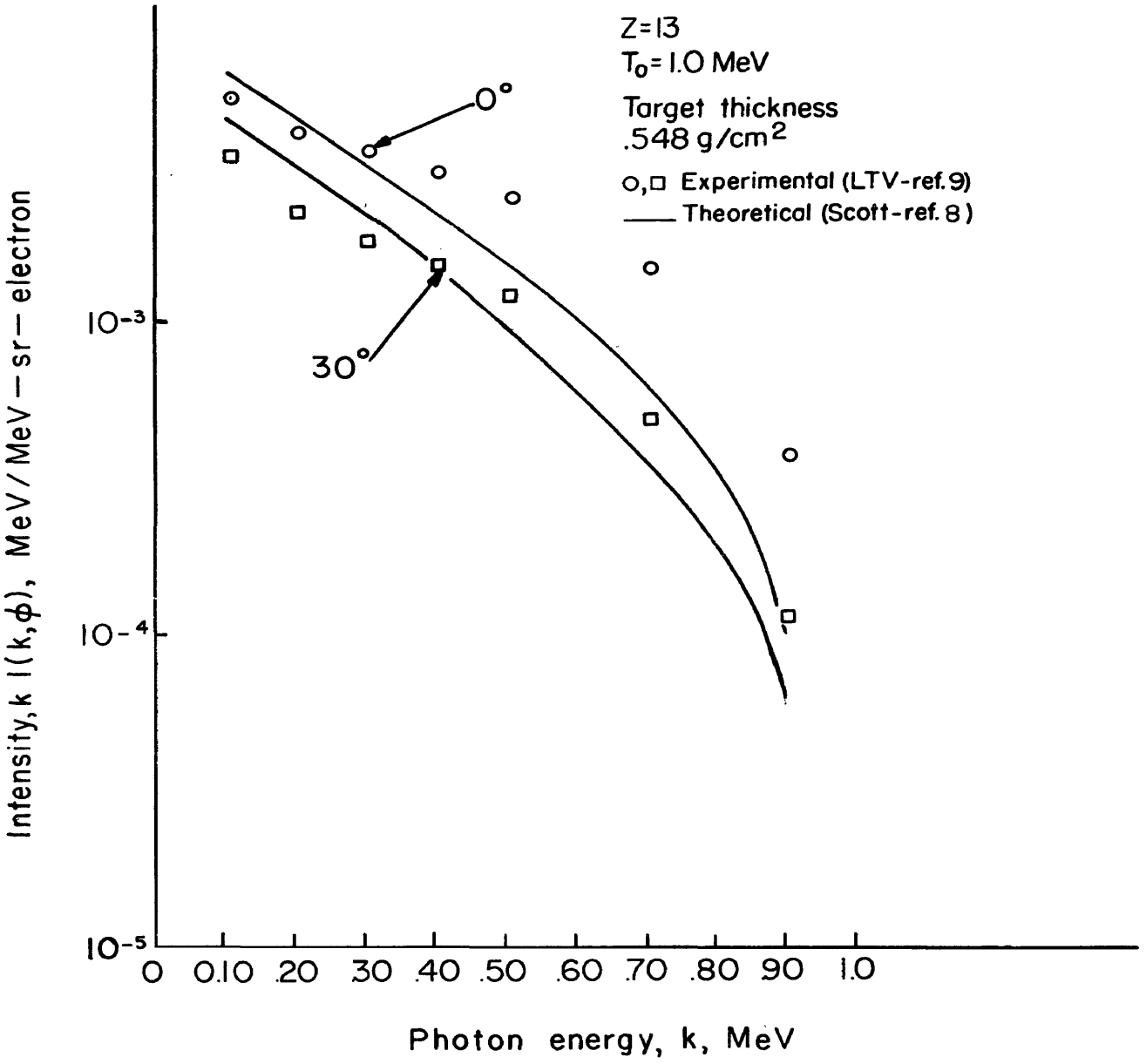

Figure 3a. - Comparison of theoretical thick target bremsstrahlung obtained by Scott (ref. 8) with experimental intensities measured by Baggerly et al (ref. 9) for aluminum at photon angles of 0° and 30° and an electron energy equal to 1 MeV.

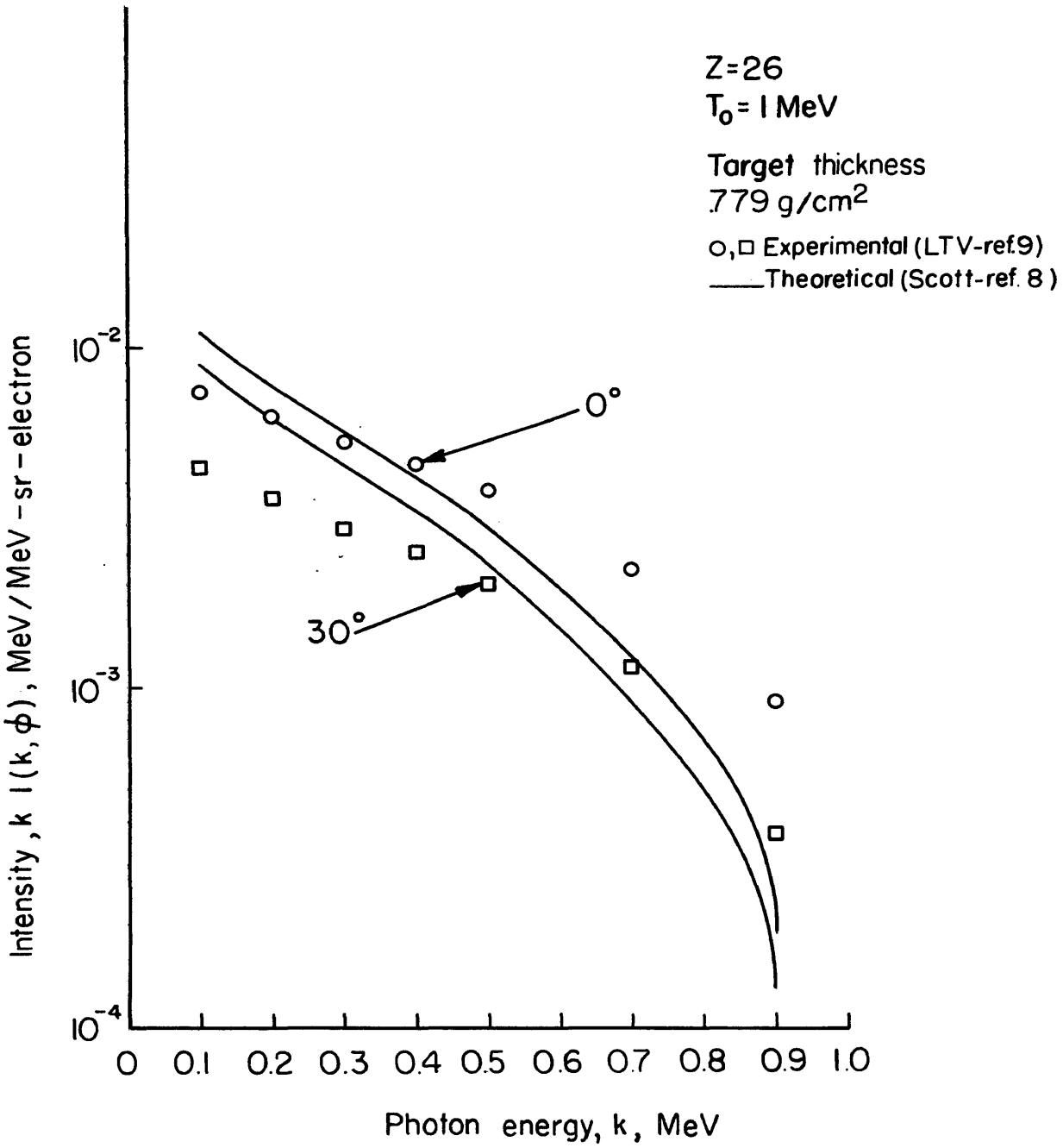

Figure 3b. - Comparison of theoretical thick target bremsstrahlung obtained by Scott (ref. 8) with experimental intensities measured by Baggerly et al (ref. 9) for iron at photon angles at 0° and 30° and an electron energy equal to 1 MeV.

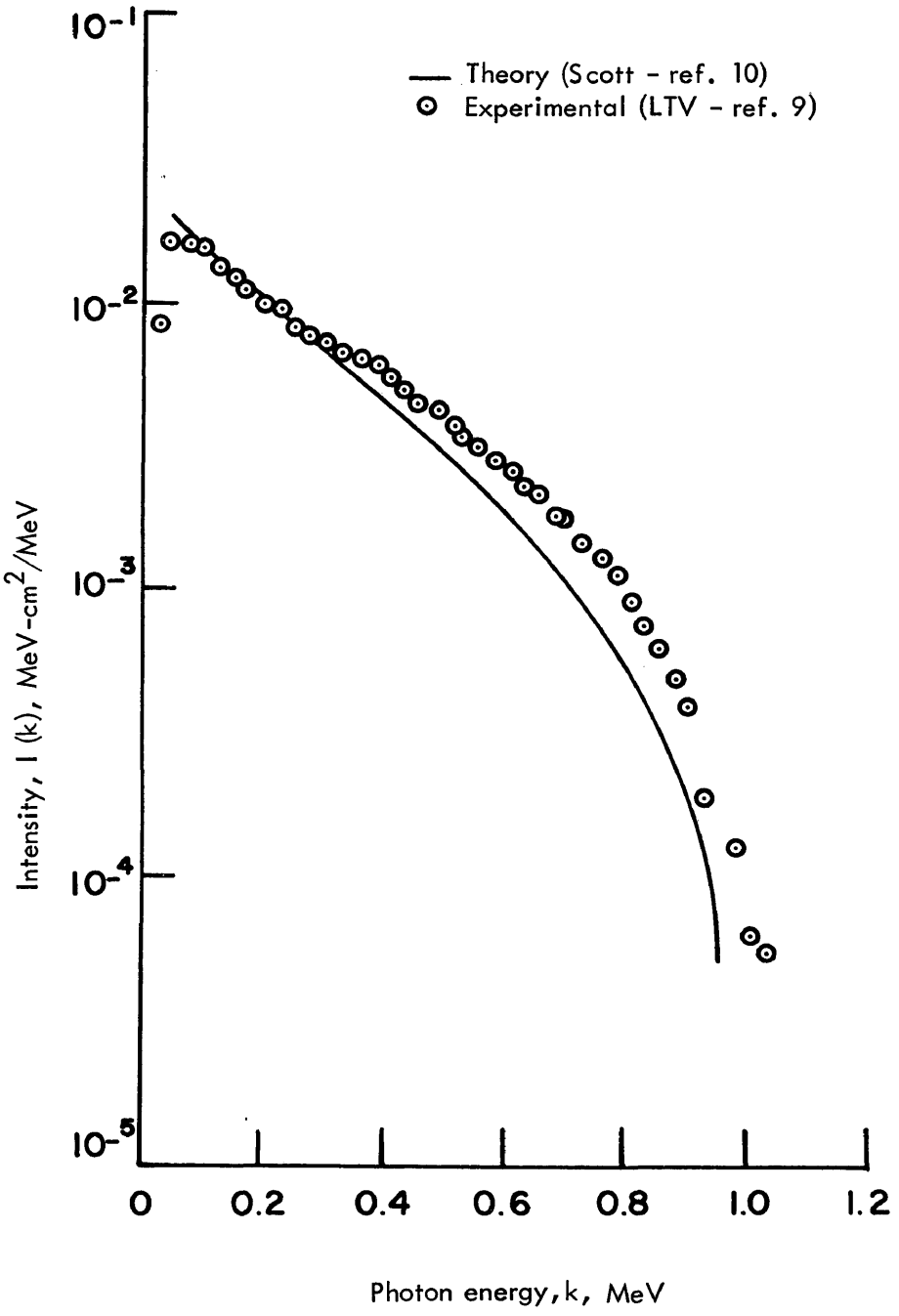

Figure 4. - Comparison of theoretical (ref. 10) and experimental photon intensities integrated over all photon angles for 1.0 MeV electrons incident on a thick aluminum target.

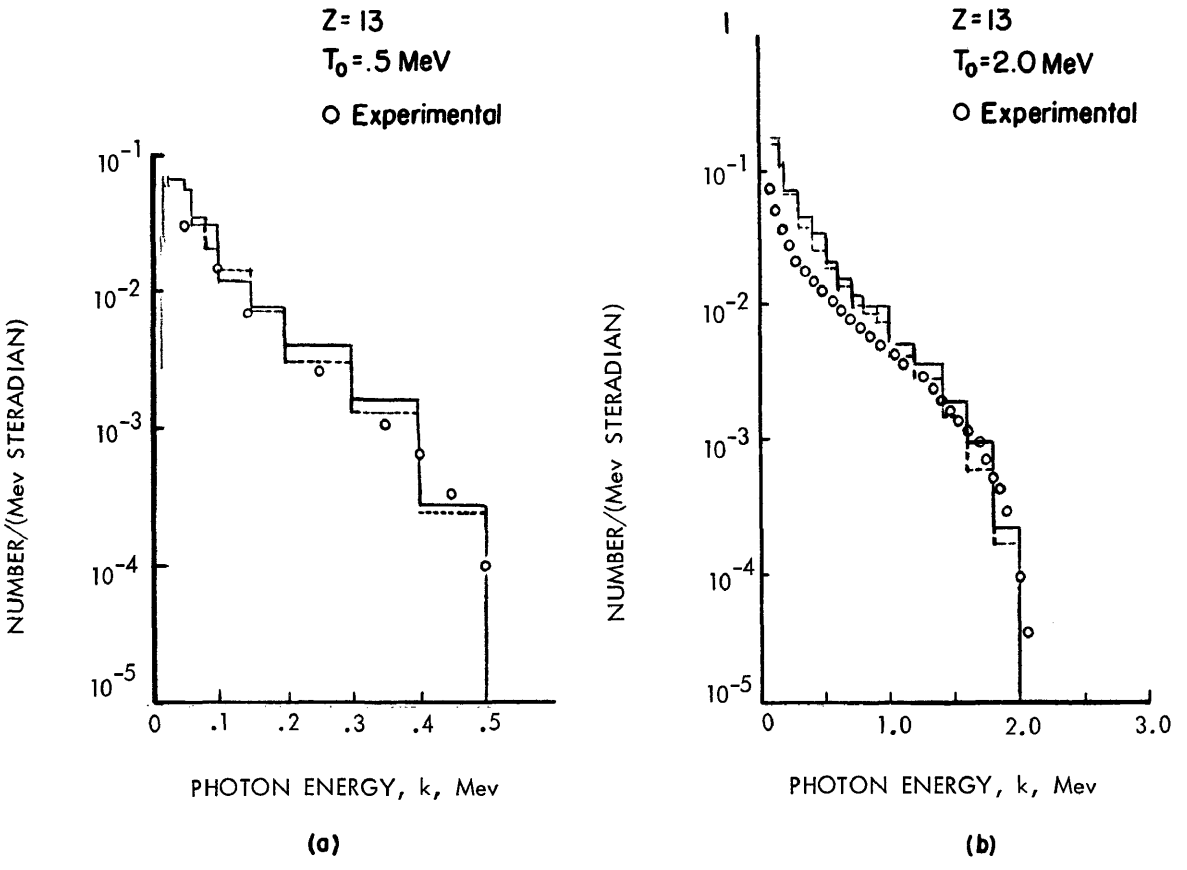

Figure 5a. - Comparison of Monte Carlo type bremsstrahlung calculation of the spectral intensity at 15° (ref. 11) with experimental data (ref. 9) for .5 MeV electrons incident on a thick aluminum target.

Figure 5b. - Comparison of Monte Carlo type bremsstrahlung calculation of the spectral intensity at 15° (ref. 11) with experimental data (ref. 9) for 2.0 MeV electrons incident on a thick aluminum target.

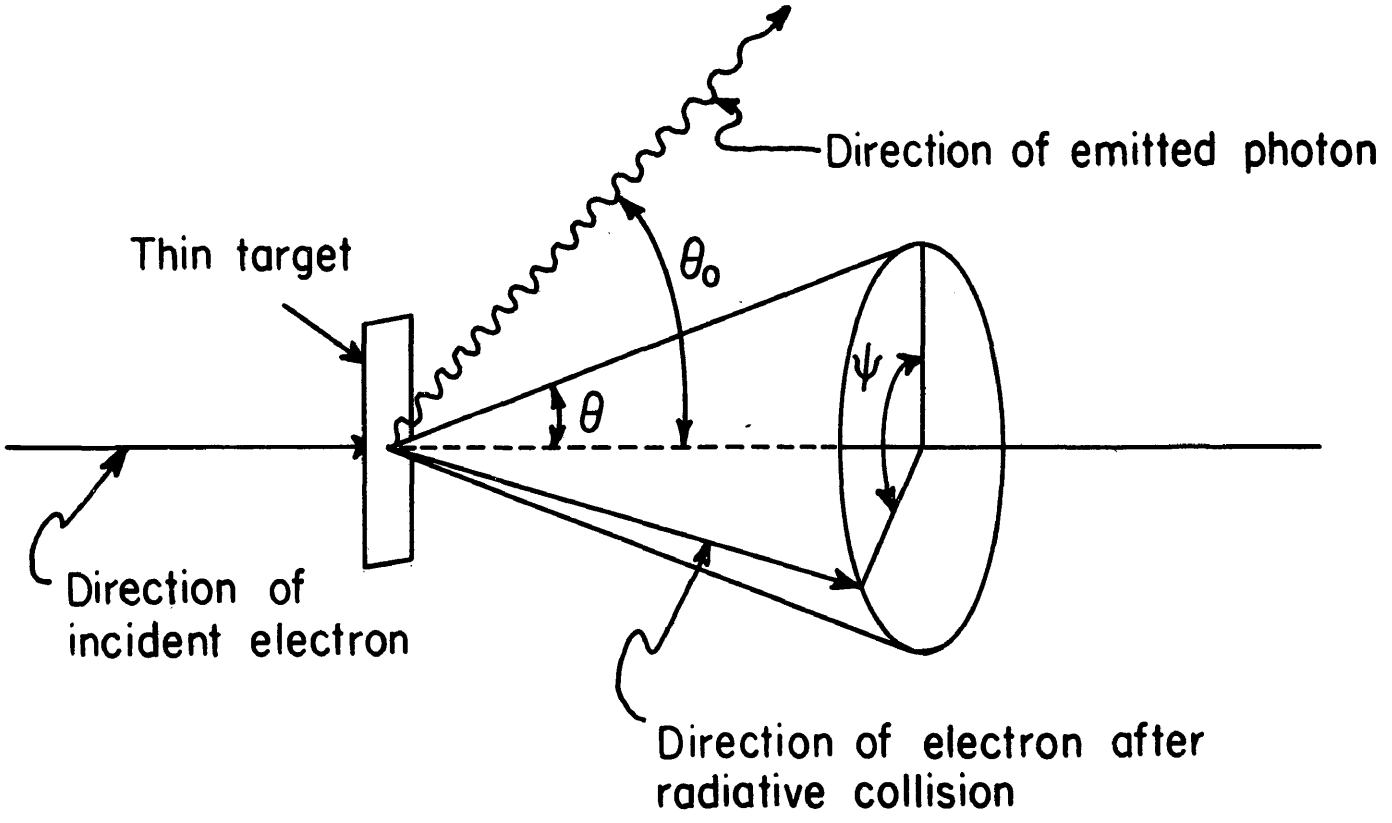

Figure 6. - Collision geometry for thin target bremsstrahlung.

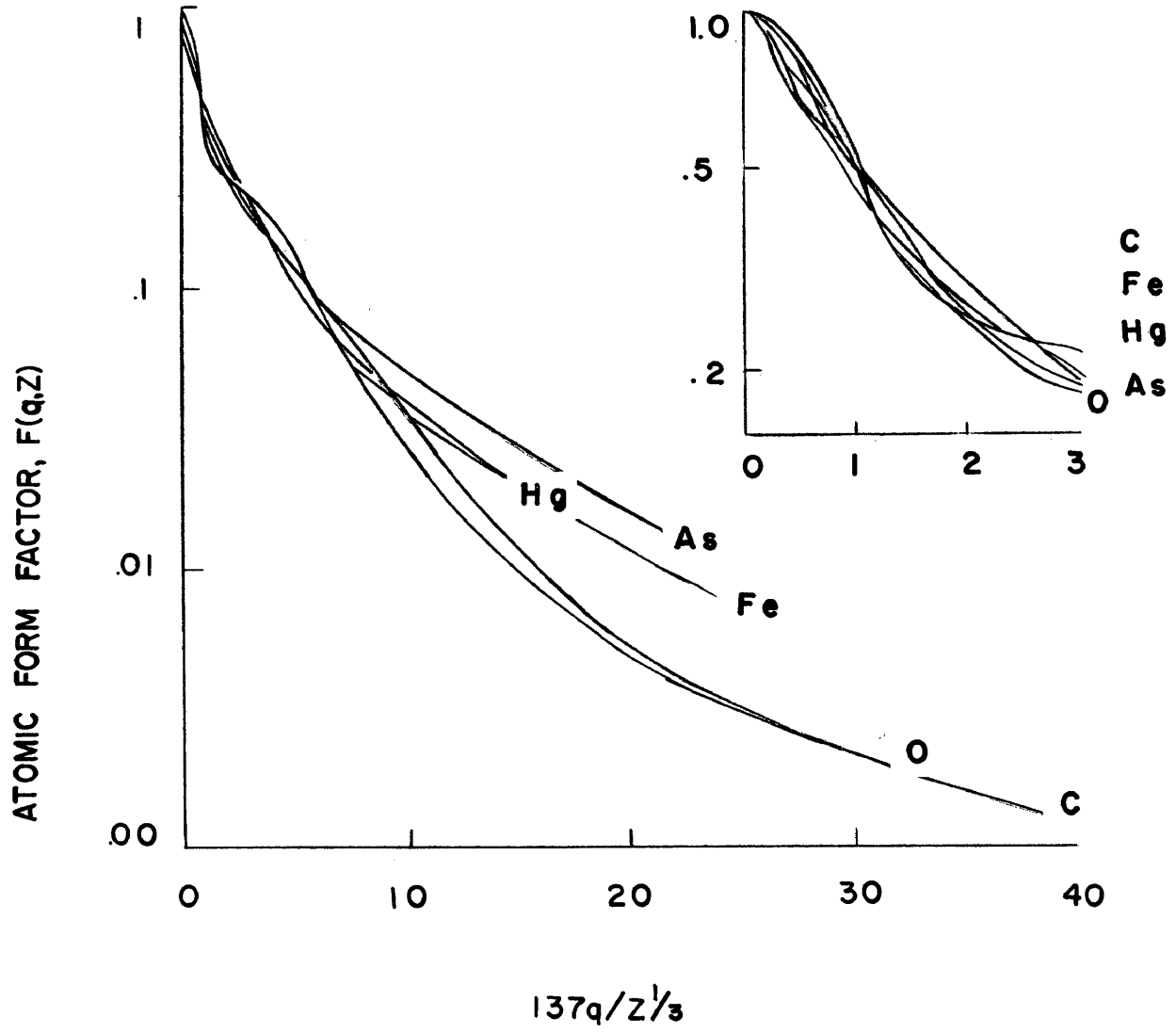

Figure 7. - Evaluation of the atomic form factor, F(q,Z) for the Hartree self-consistent field model as a function of the nuclear momentum transfer, q (from ref. 14).

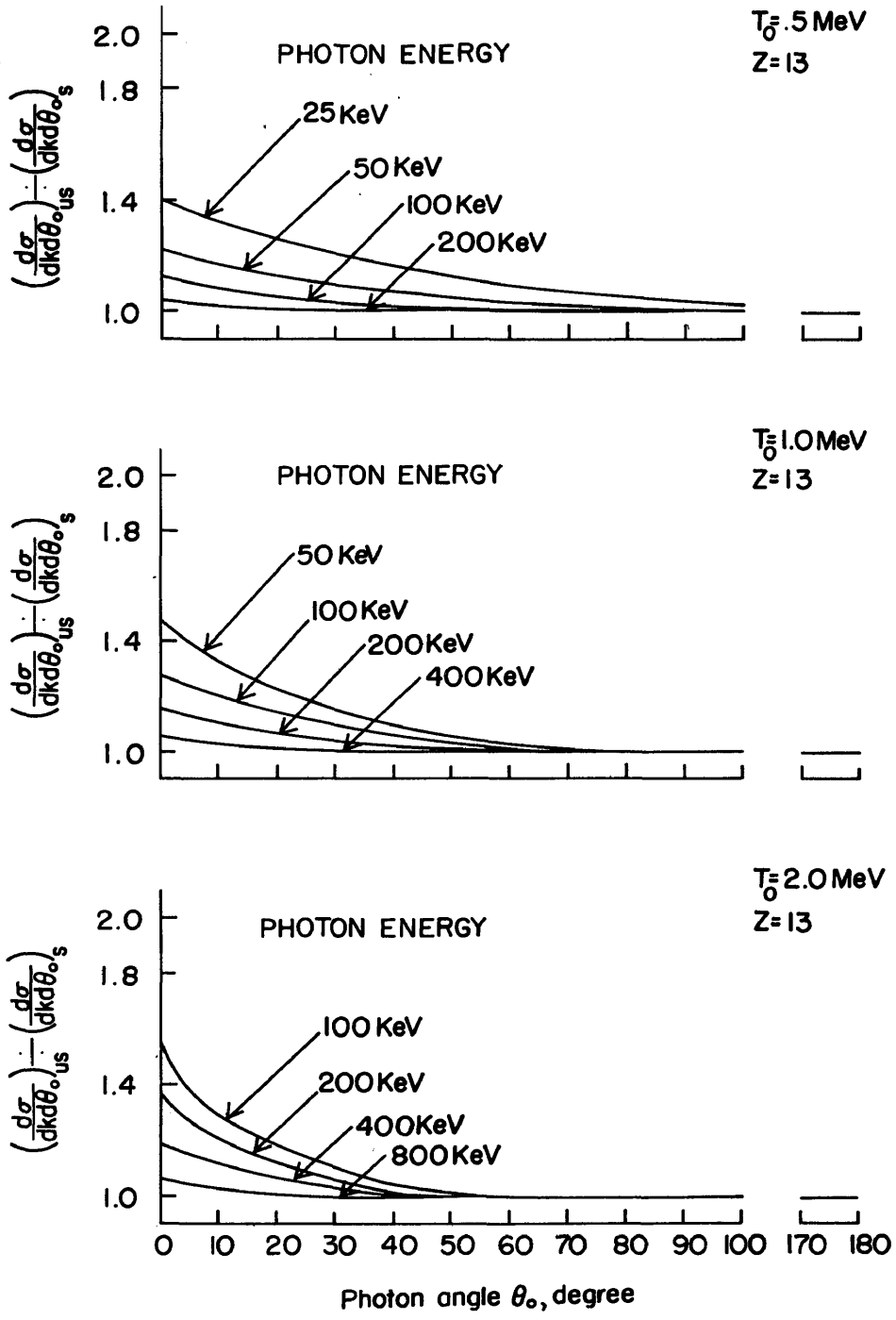

Figure 8a. - The ratio of the unscreened (Equation 3.09) and the screened (Equation 3.11) thin target bremsstrahlung cross sections for aluminum at electron energies of 0.5, 1.0, and 2.0 MeV.

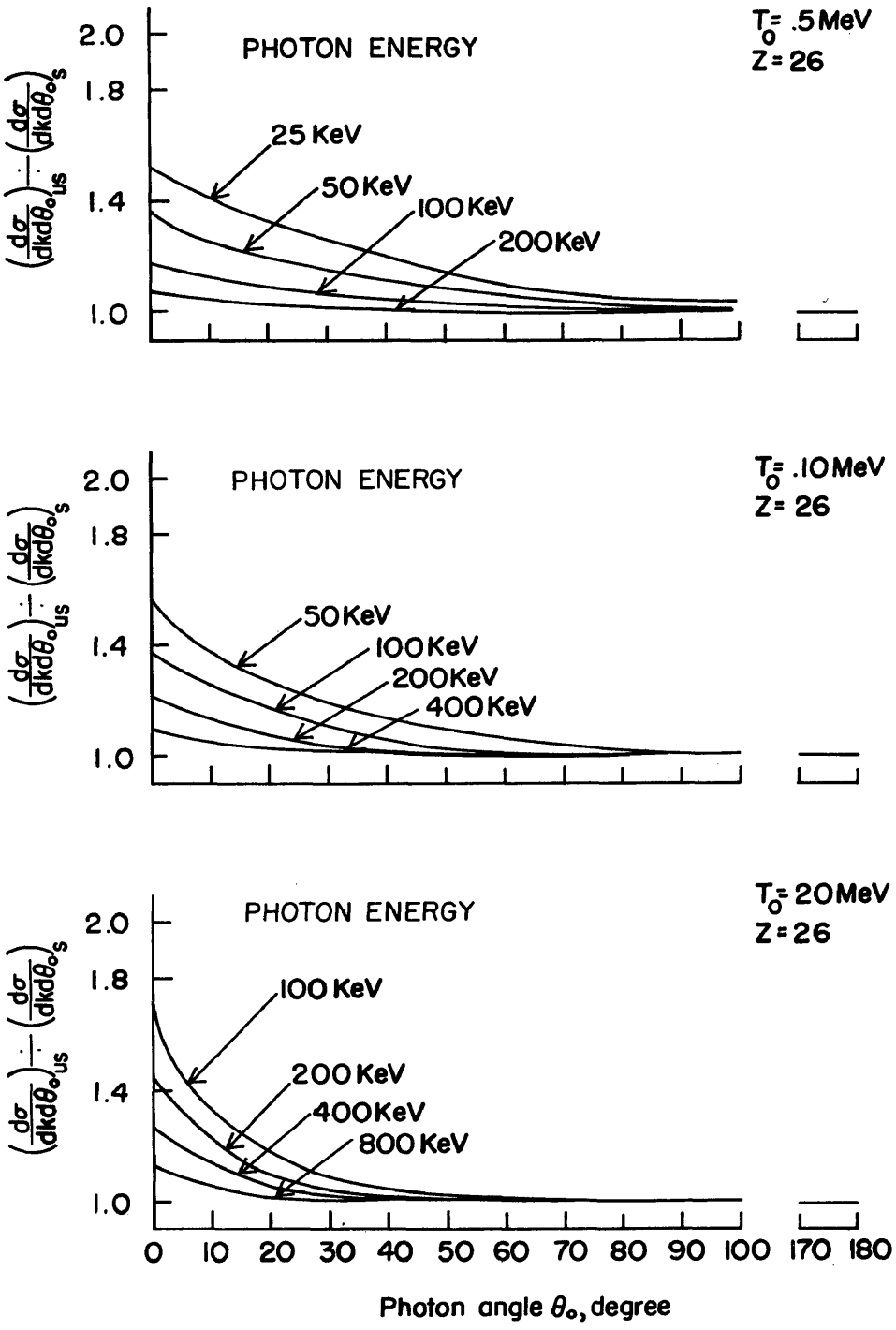

Figure 8b. - The ratio of the unscreened (Equation 3.09) and the screened (Equation 3.11) thin target bremsstrahlung cross sections for iron at electron energies of 0.5, 1.0, and 2.0 MeV.

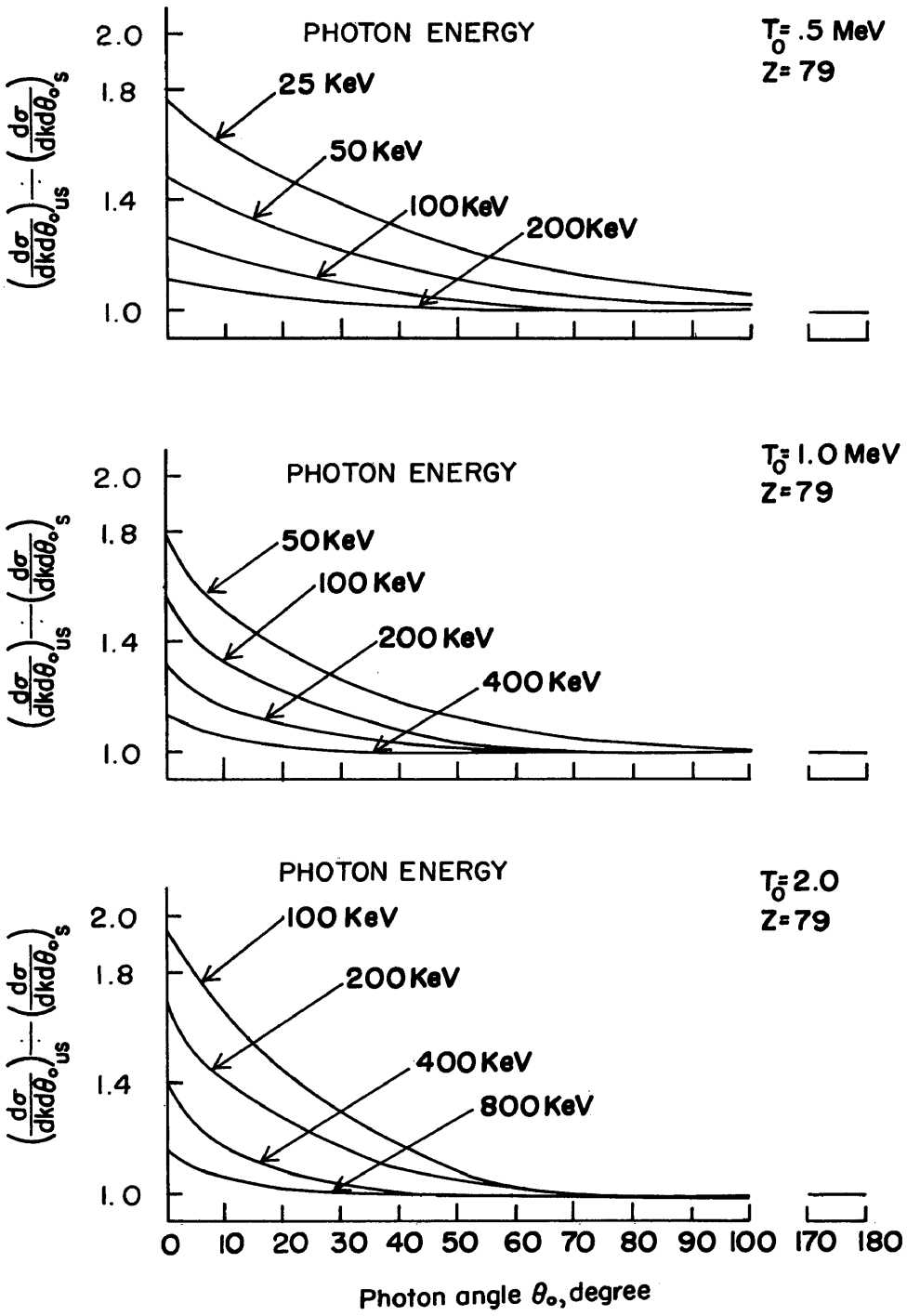

Figure 8c. - The ratio of the unscreened (Equation 3.09) and the screened (Equation 3.11) thin target bremsstrahlung cross sections for gold at electron energies of 0.5, 1.0, and 2.0 MeV.

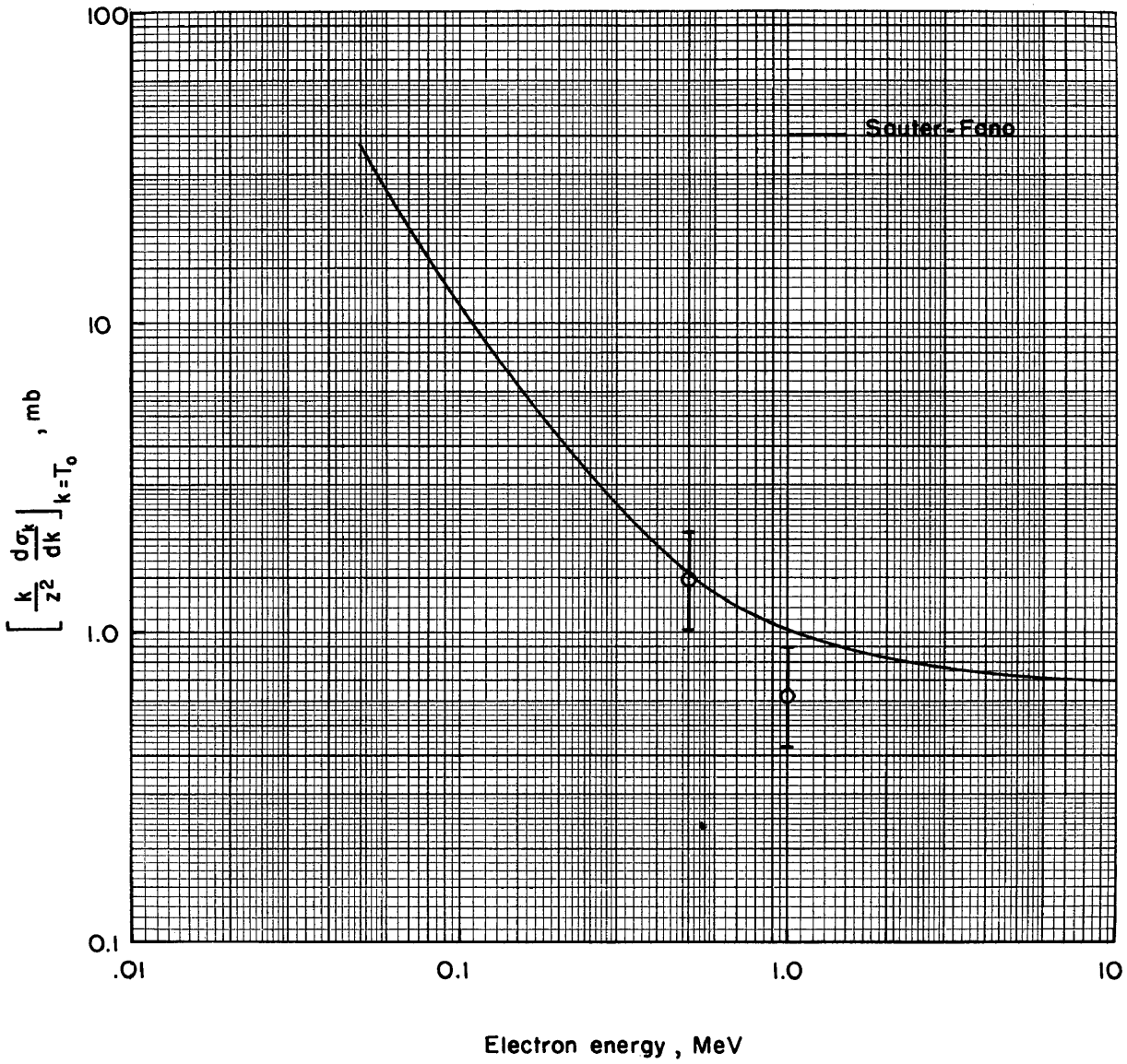

Figure 9. - Comparison of theoretical and experimental thin target bremsstrahlung cross sections at the high-frequency limit for aluminum.

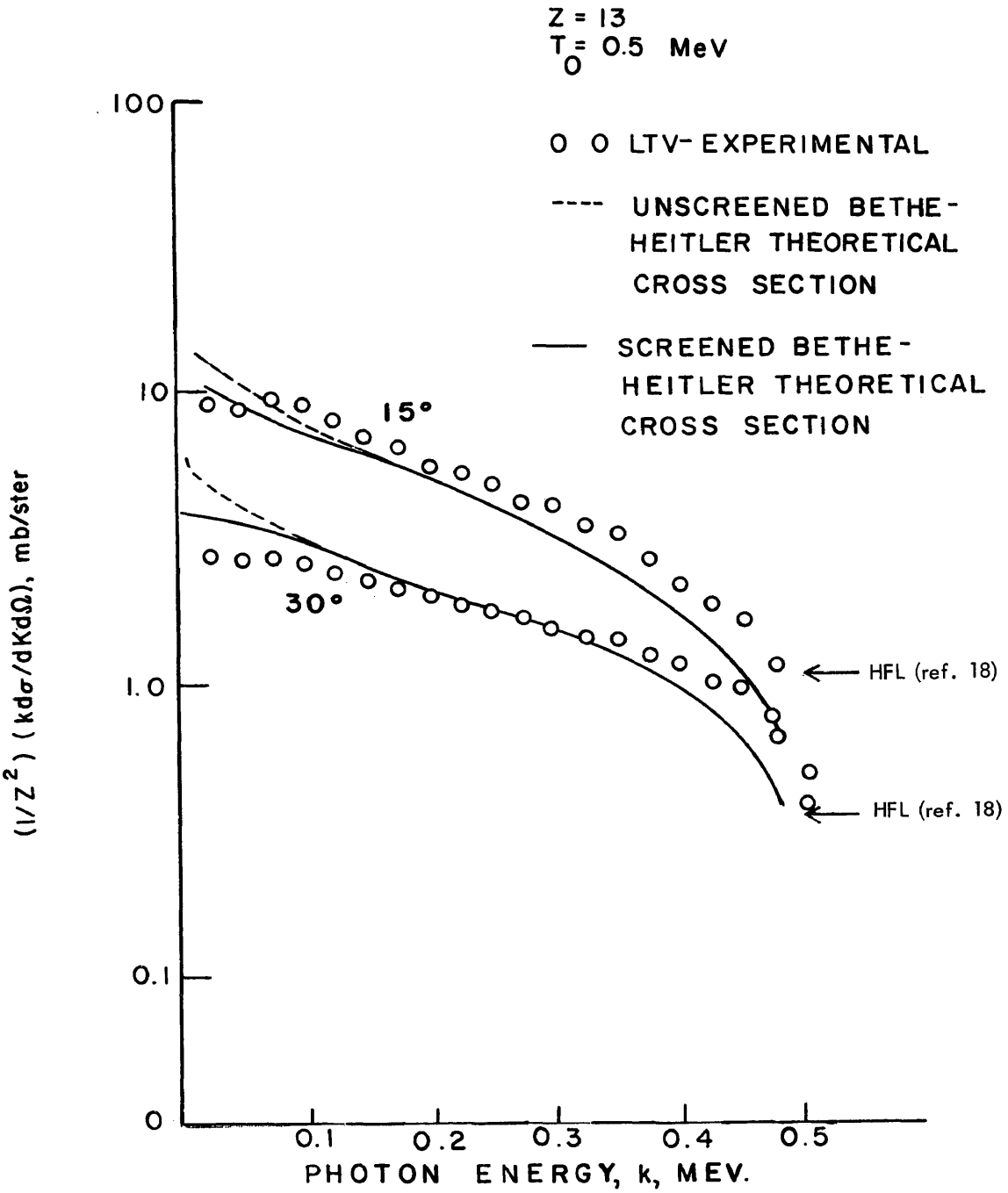

Figure 10a. - Comparison of screened and unscreened Beth-Heitler theoretical cross sections and the high frequency limit (HFL) cross sections with experimental thin target cross sections for aluminum at photon angles of 15° and 30° and on electron energy equal to .5 MeV.

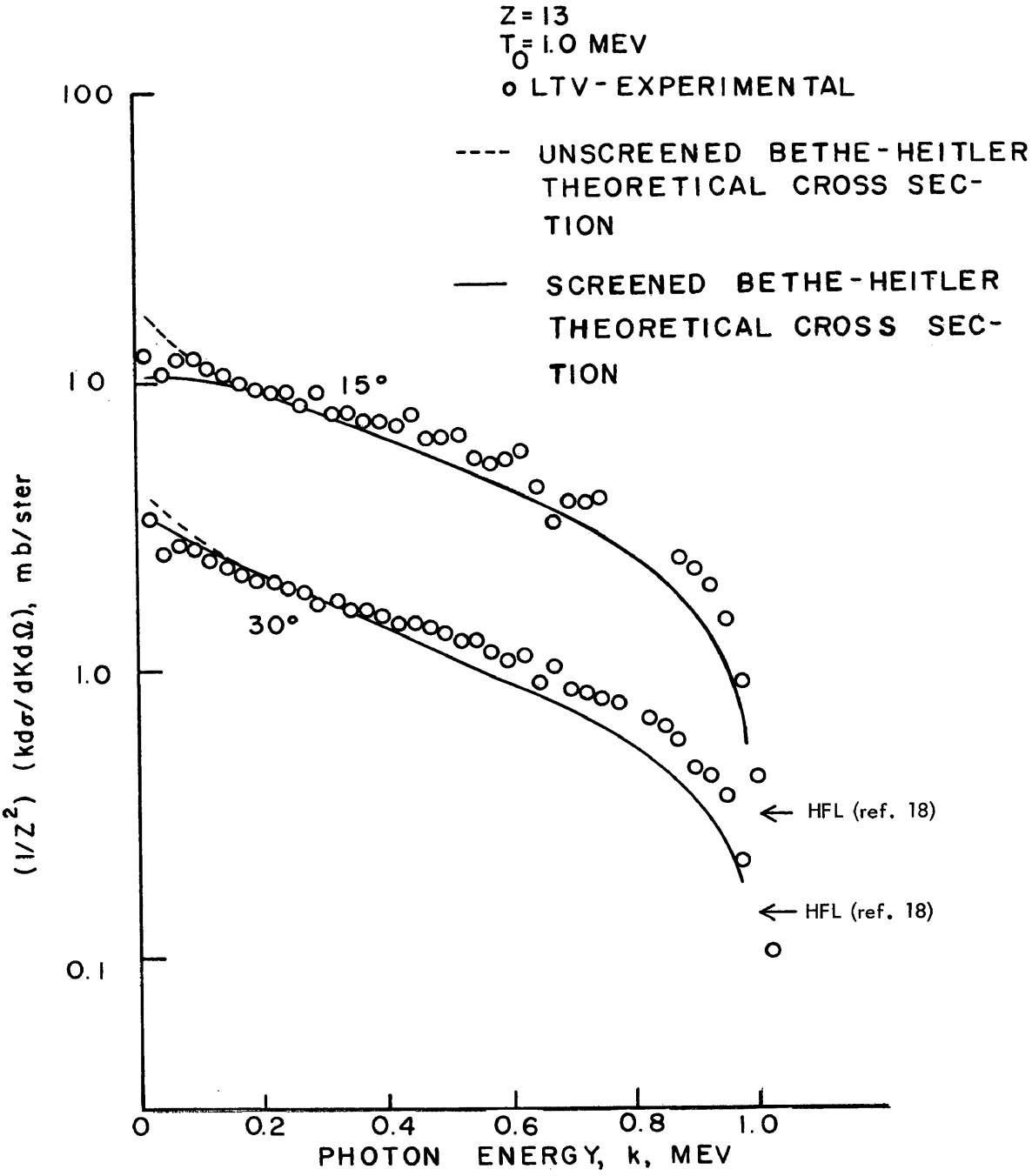

Figure 10b. - Comparison of the screened and unscreened Beth-Heitler theoretical cross sections and the high frequency limit HFL cross section with experimental thin target cross section at photon angles of 15° and 30° and an electron energy equal to 1.0 MeV.

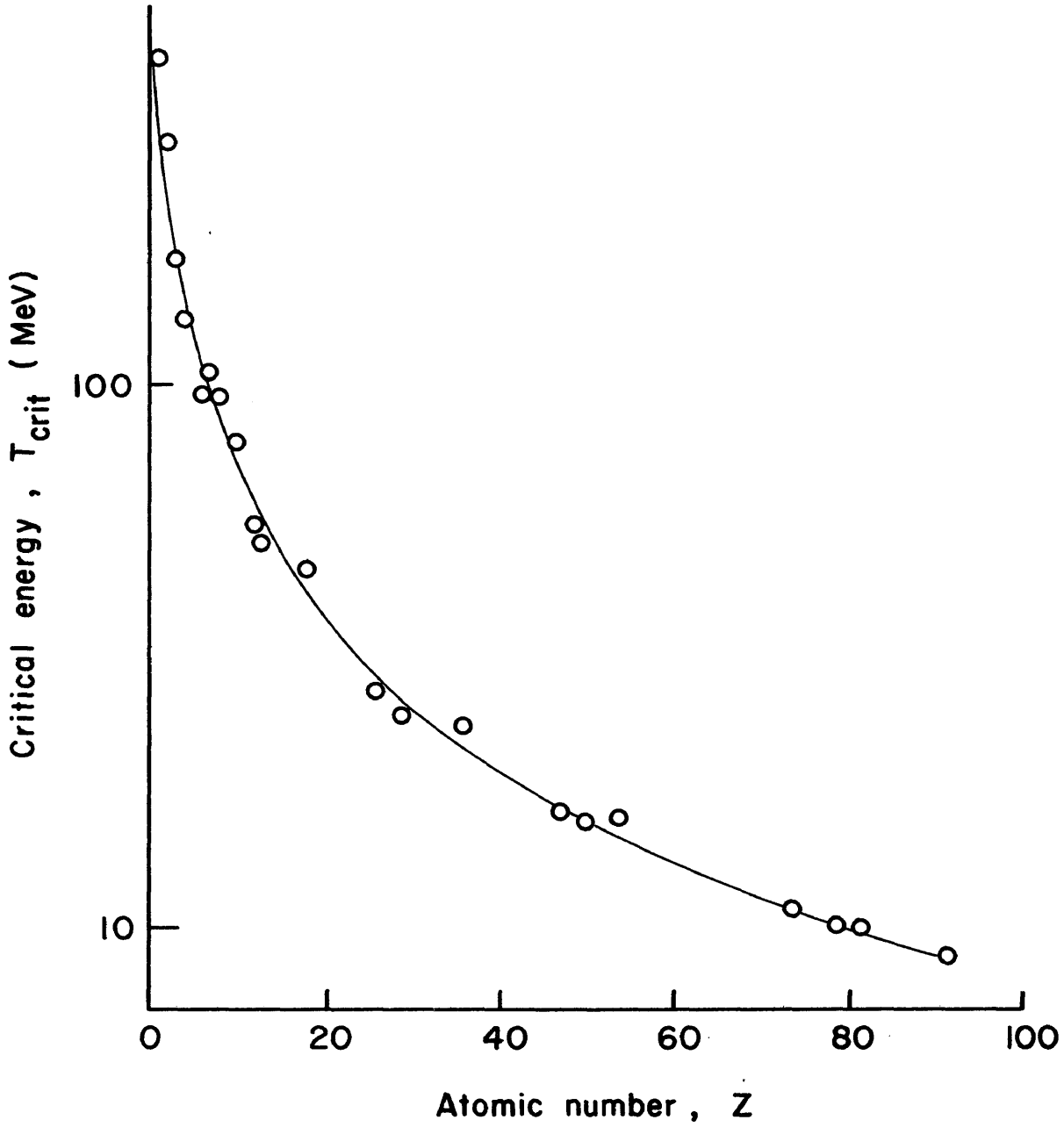

Figure 11. - Critical energy for electrons al as a function of atomic number (from ref. 19).

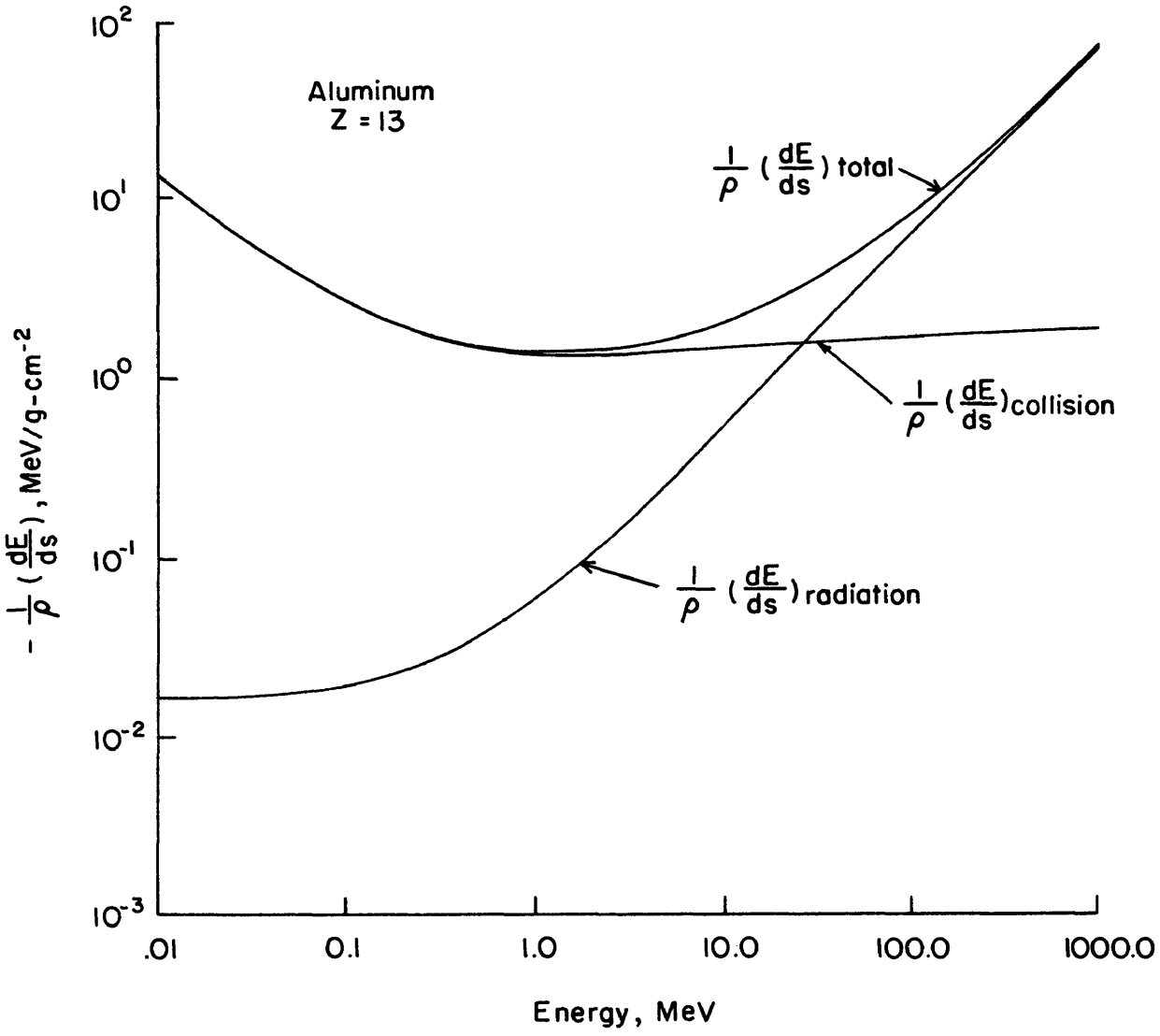

Figure 12a. - The mean ionization loss, the mean radiative loss, and the total stopping power for aluminum for electrons in the energy range from .01 MeV to 1000 MeV.

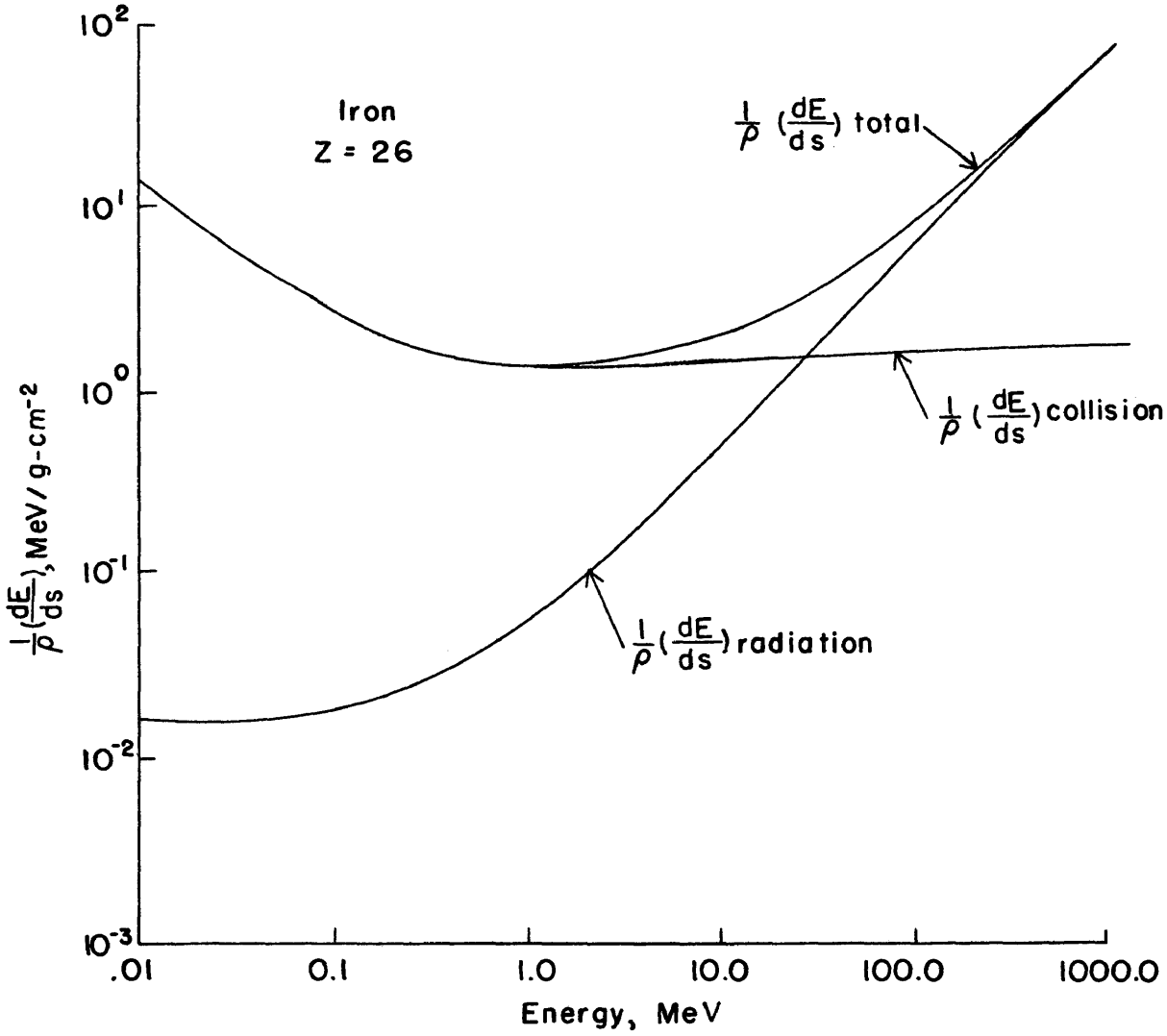

Figure 12b. - The mean ionization loss, the mean radiative loss, and the total stopping power for iron for electrons in the energy range from .01 MeV to 1000 MeV.

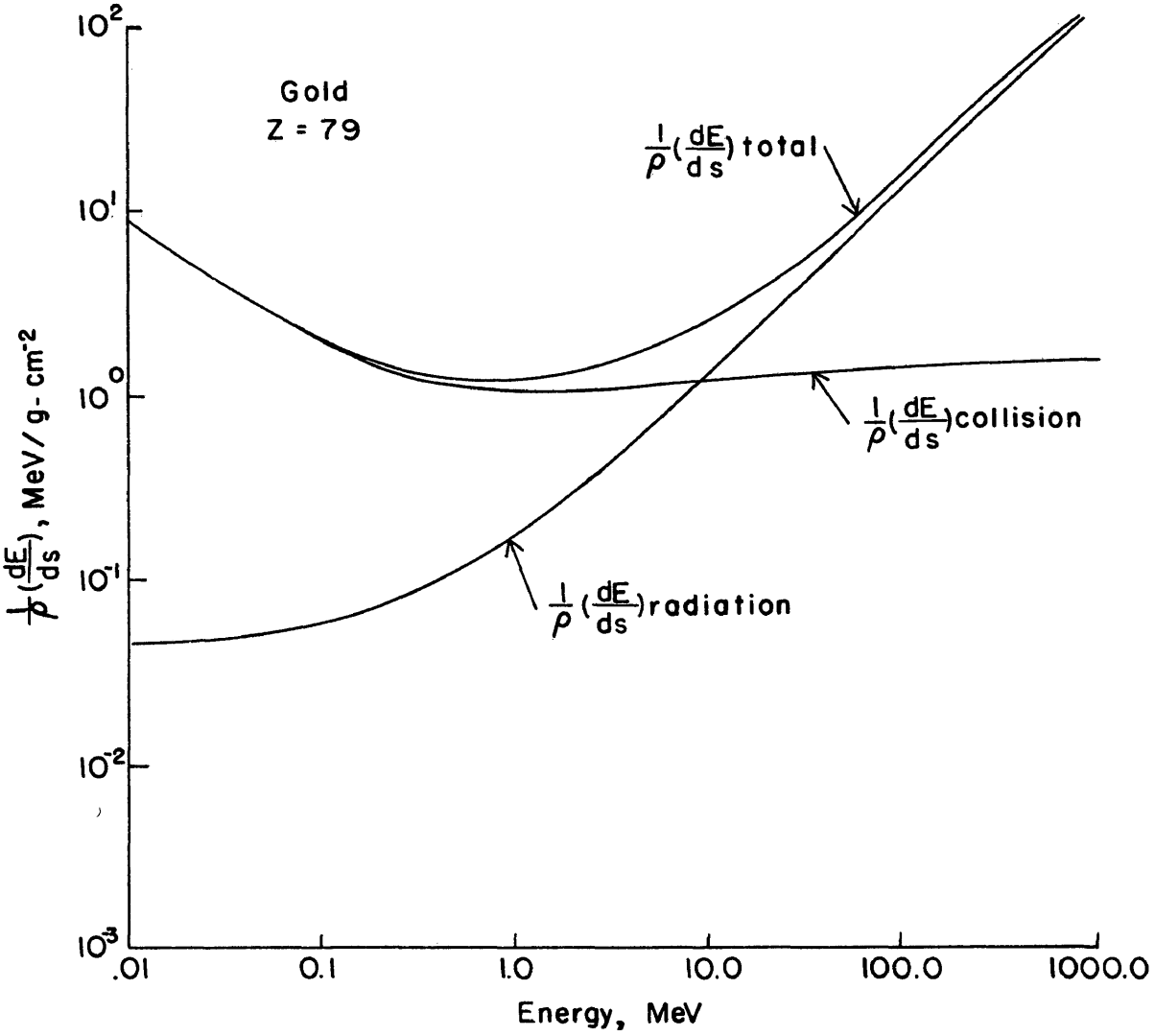

Figure 12c. - The mean ionization loss, the mean radiative loss, and the total stopping power for gold for electrons in the energy range from .01 MeV to 1000 MeV.

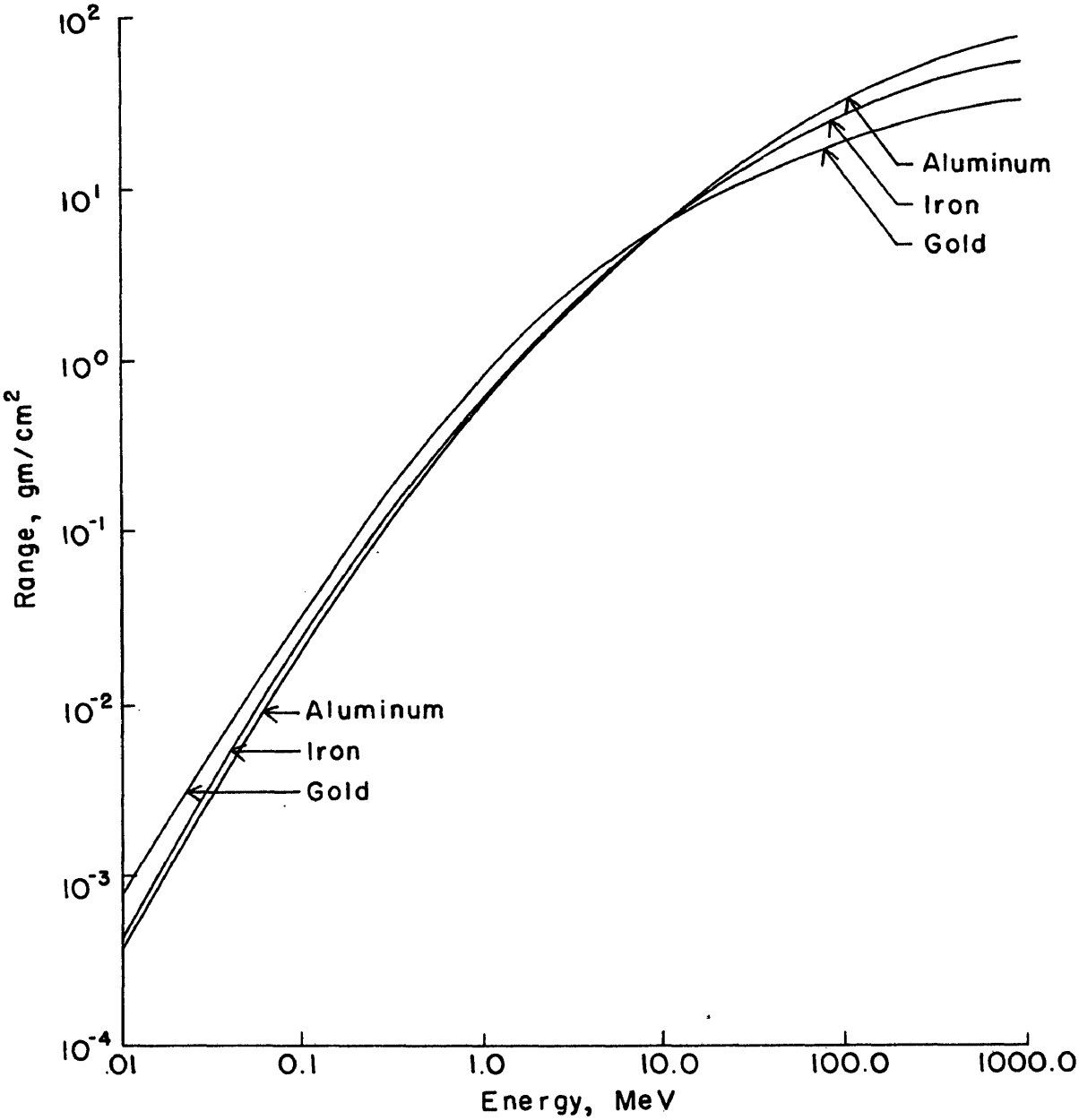

Figure 13. - The mean range of electrons in the energy range from .01 MeV to 1000 MeV in aluminum, iron, and gold.

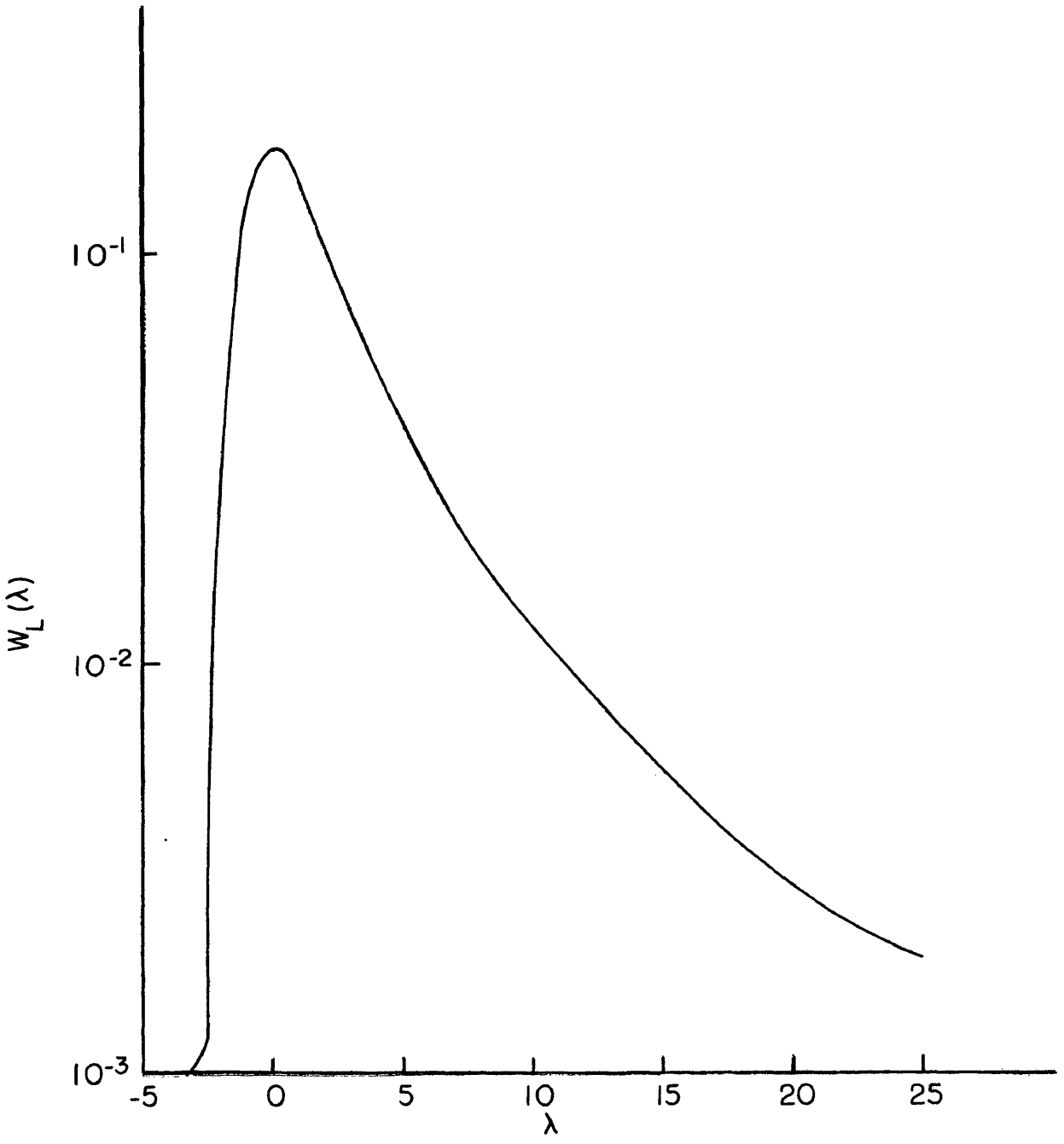

Figure 14. - Graph of Landau function $W_L(\lambda)$ (from ref. 23).

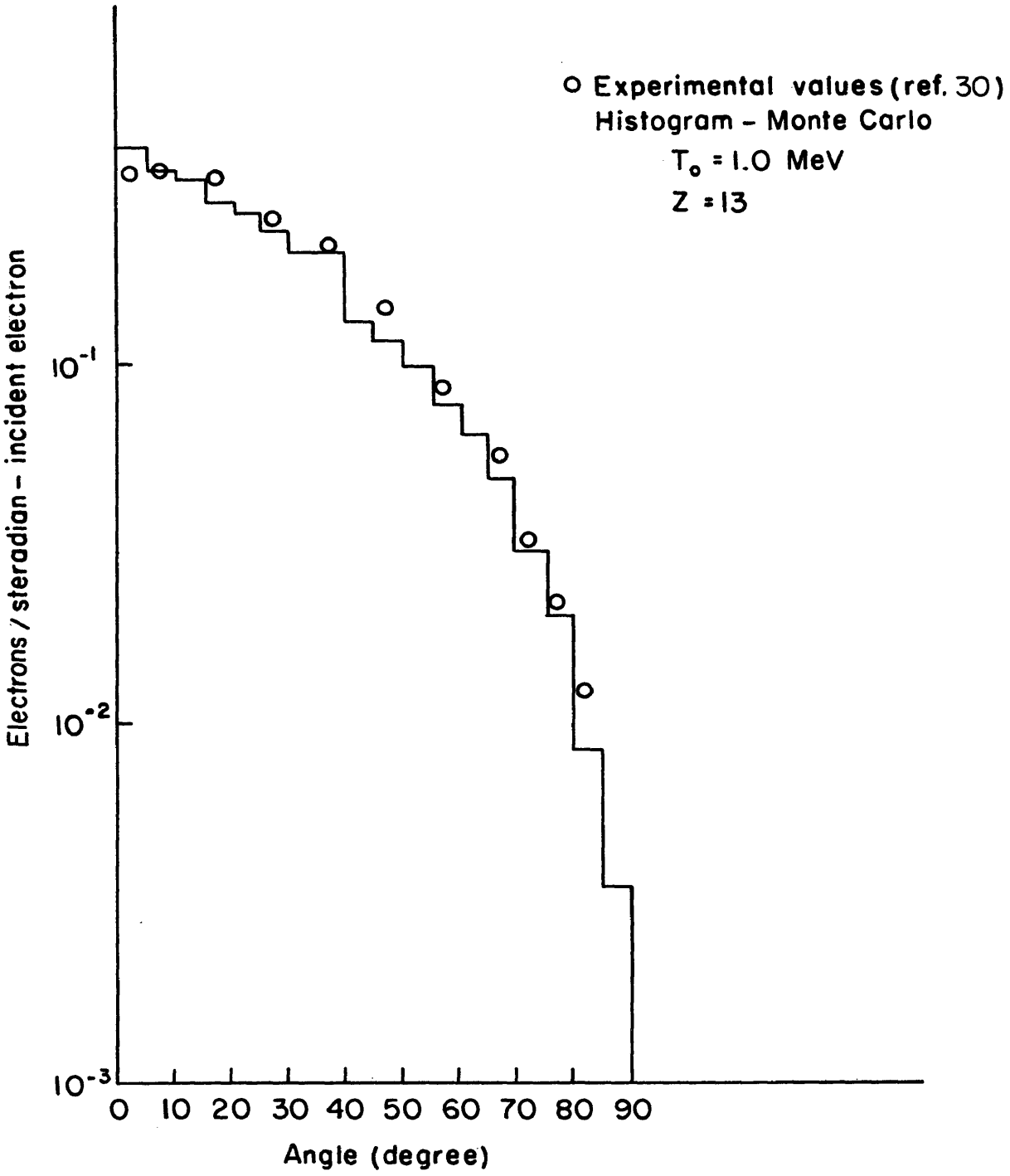

Figure 15a.- Comparison of theoretical and experimental distribution of 1.0 MeV electrons transmitted through an aluminum target of thickness equal to .11 gm/cm^2.

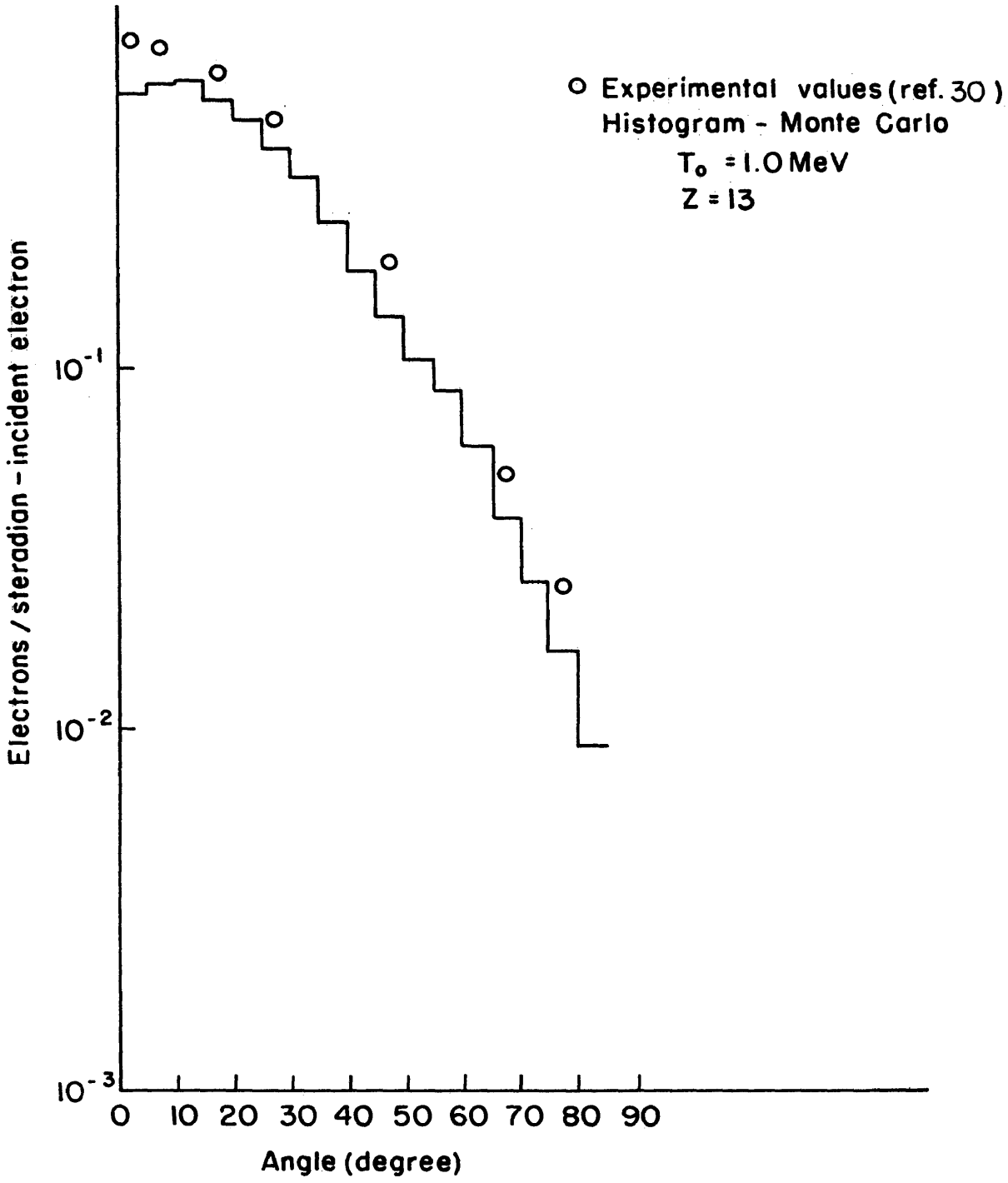

Figure 15b. - Comparison of theoretical and experimental distribution of 1.0 MeV electrons transmitted through an aluminum target of thickness equal to .22 gm/cm^2.

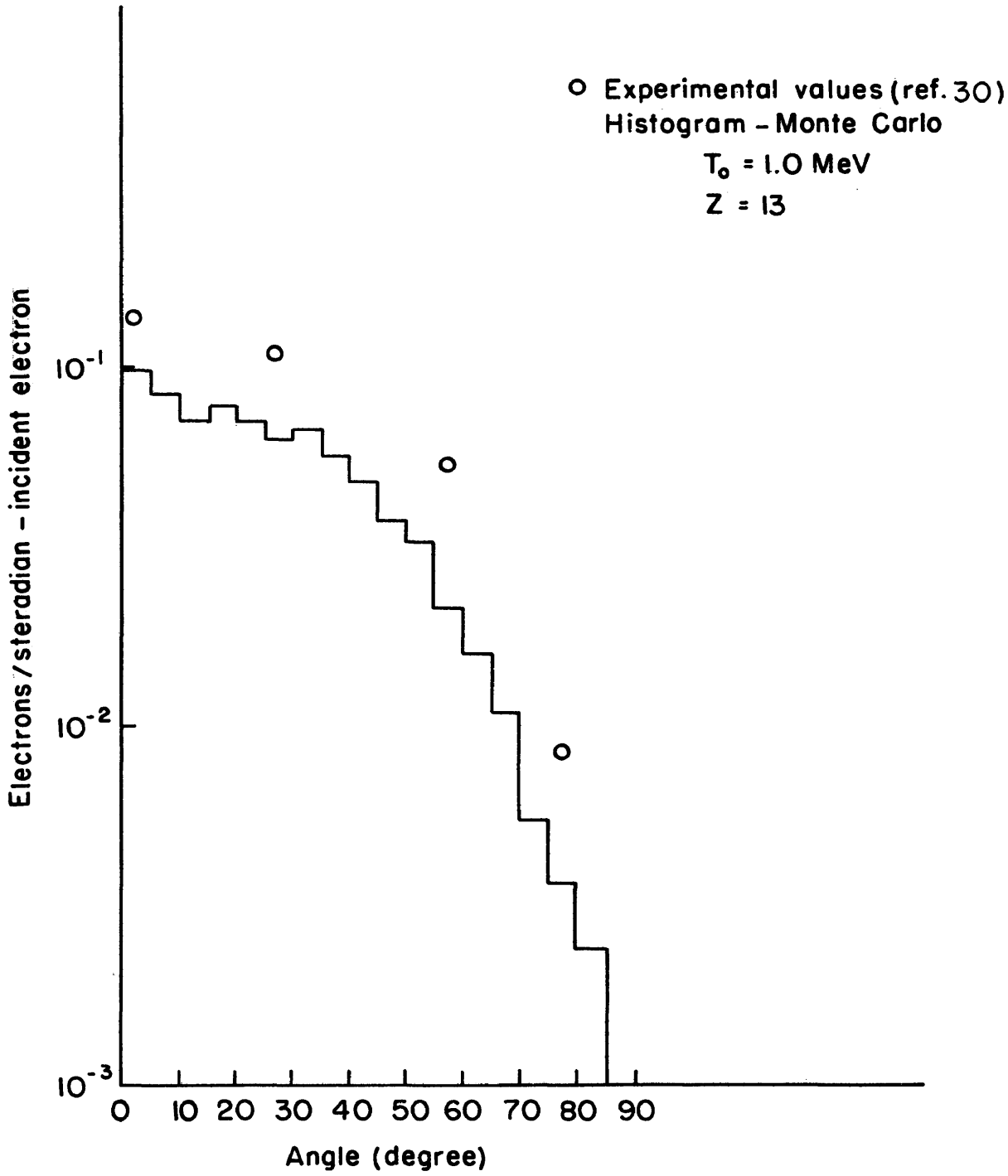

Figure 15c. - Comparison of theoretical and experimental distribution of 1.0 MeV electrons transmitted through an aluminum target of thickness equal to .22 gm/cm^2.

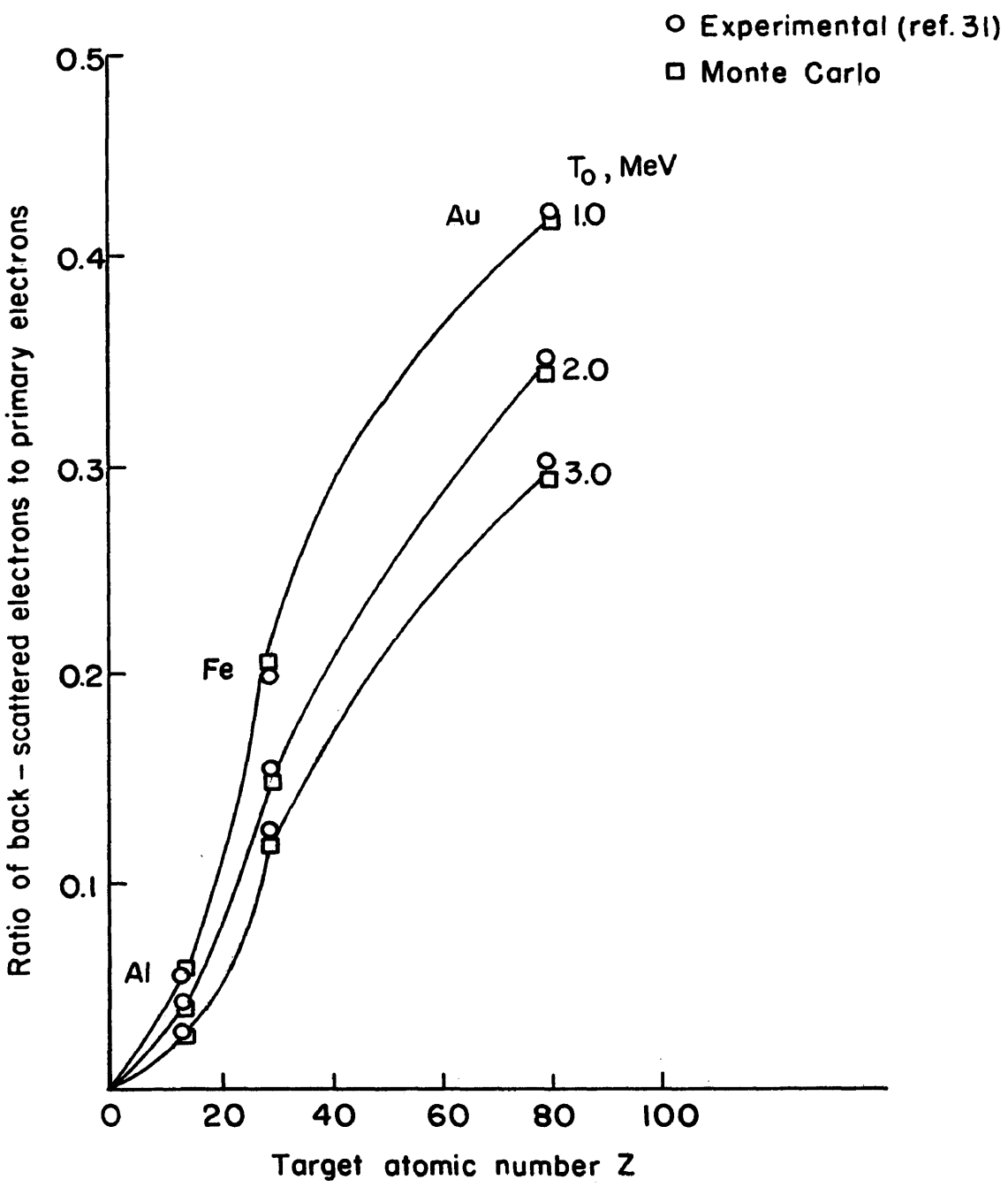

Figure 16. - Comparison of fractional number of backscattered electrons calculated from Monte Carlo program and experimental data for 1 MeV electron.

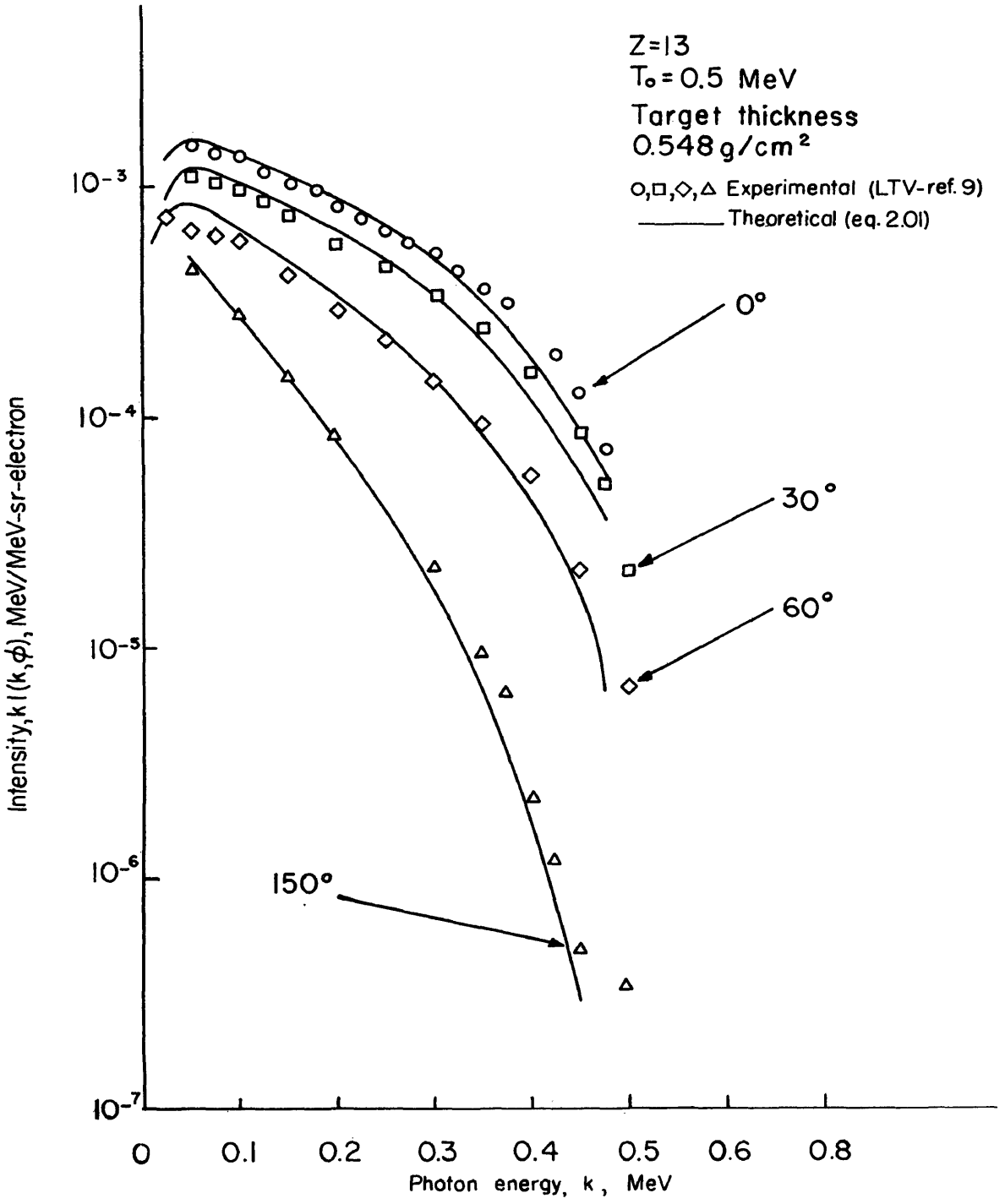

Figure 17. - Comparison of theoretical and experimental bremsstrahlung spectral intensities at photon angles of 0°, 30°, 60°, and 150° for .5 MeV electrons incident on a thick aluminum target.

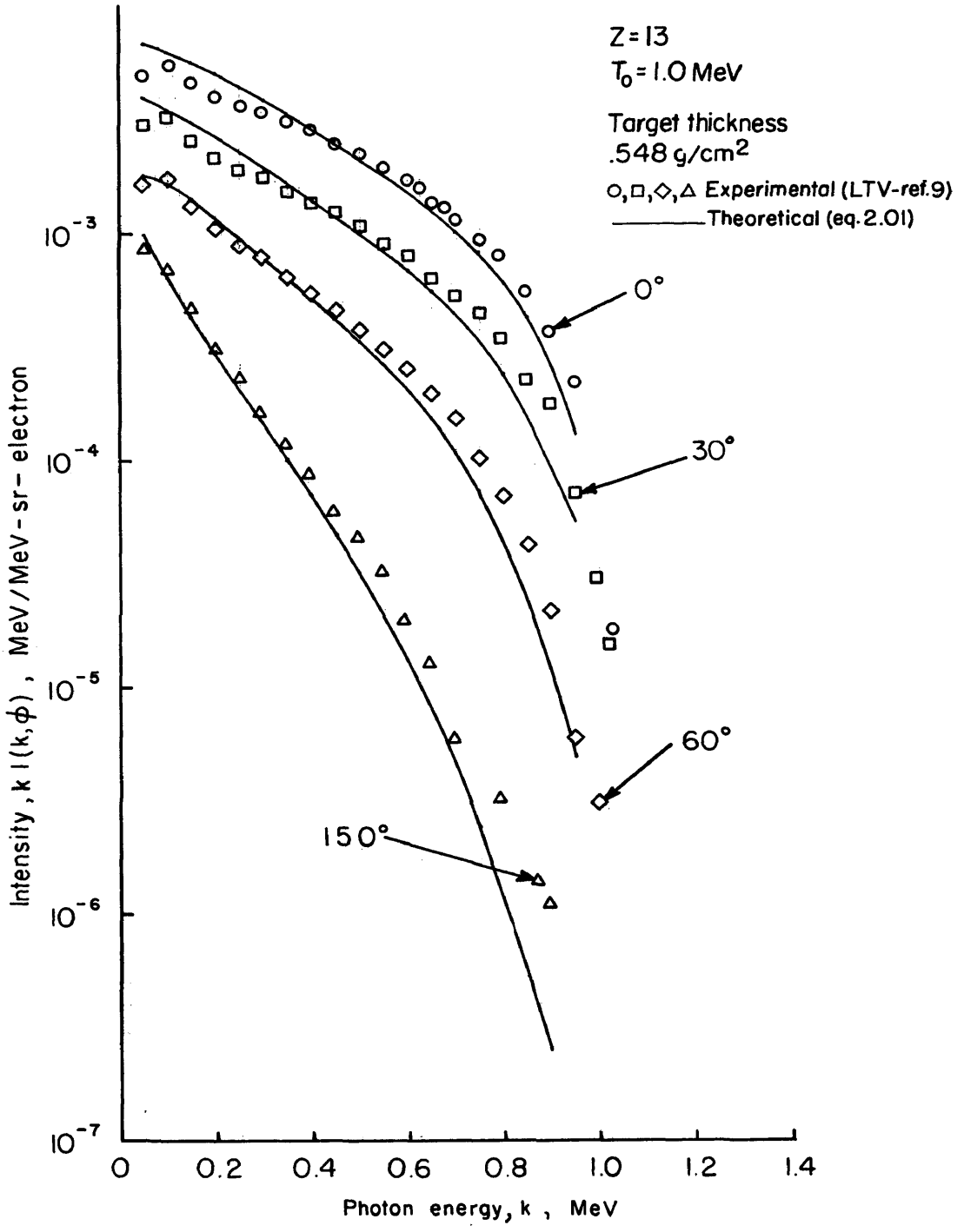

Figure 18. - Comparison of theoretical and experimental bremsstrahlung spectral intensities at photon angles of 0°, 30°, 60°, and 150° for 1.0 MeV electrons incident on a thick aluminum target.

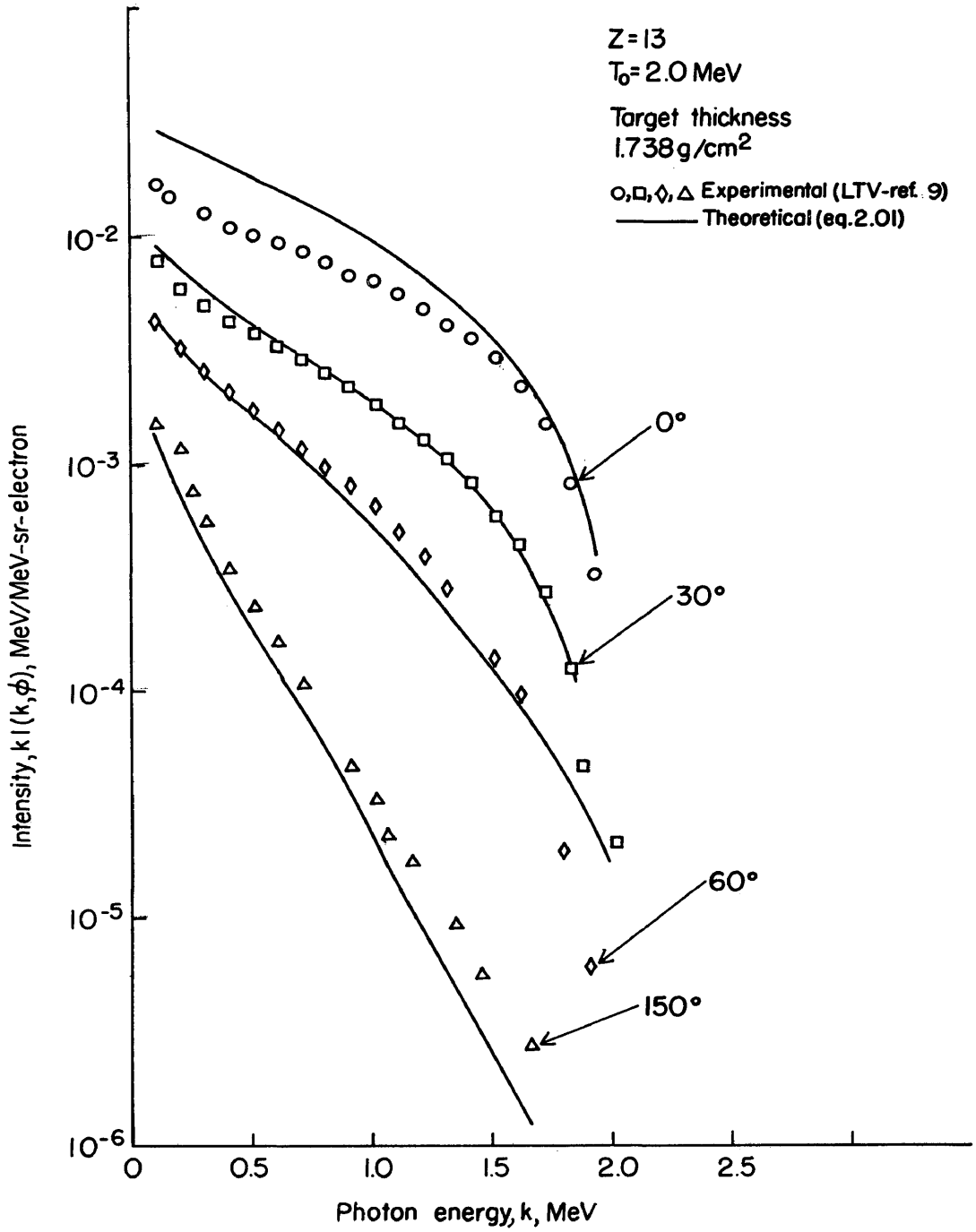

Figure 19. - Comparison of the theoretical and experimental bremsstrahlung spectral intensities at photon angles of 0°, 30°, 60°, and 150° for 2.0 MeV electrons incident on a thick aluminum target.

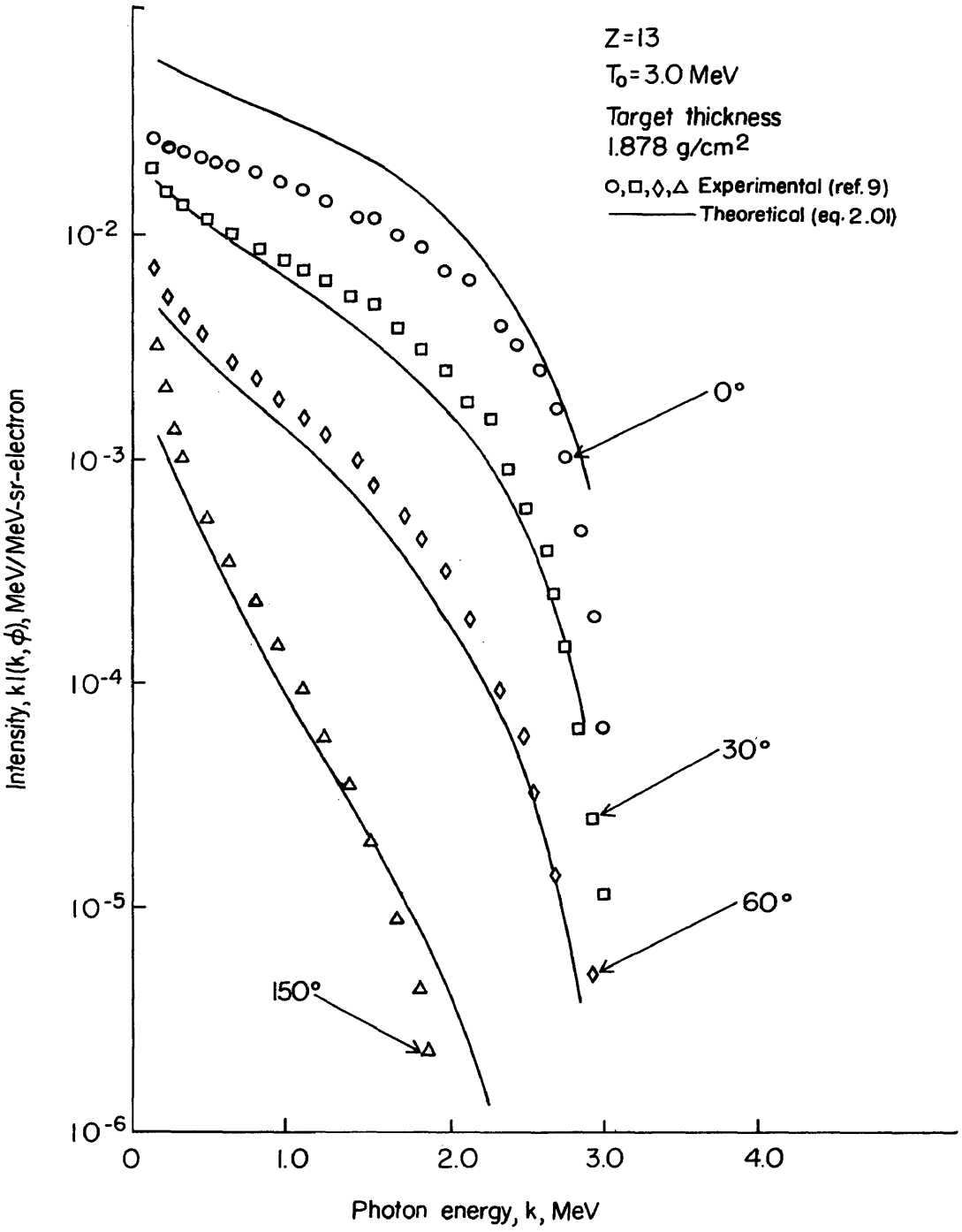

Figure 20. - Comparison of the theoretical and experimental bremsstrahlung spectral intensities at photon angles of 0°, 30°, 60°, and 150° for 3.0 MeV electrons incident on a thick aluminum target.

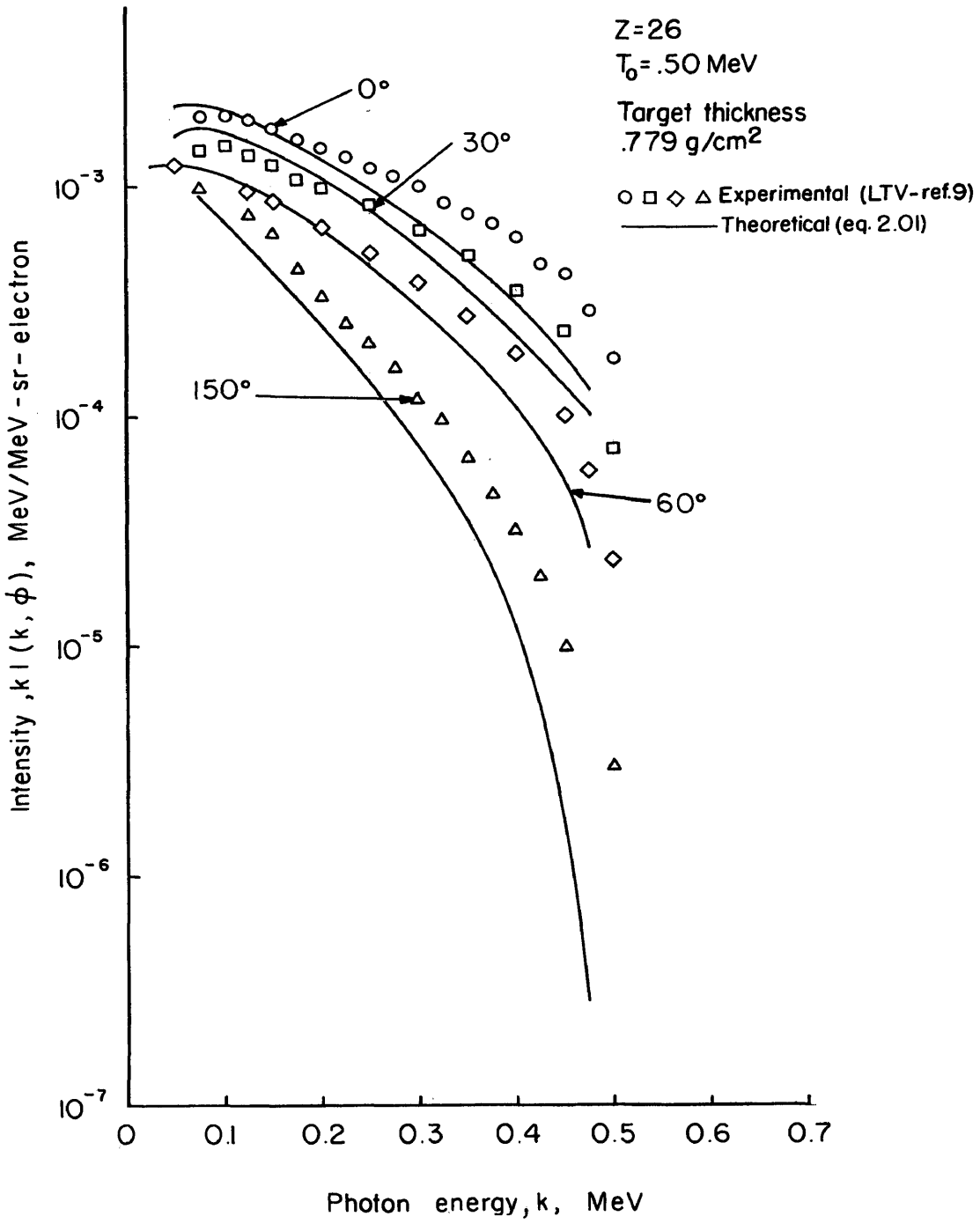

Figure 21. - Comparison of the theoretical and experimental bremsstrahlung spectral intensities at photon angles of 0°, 30°, 60°, and 150° for .5 MeV electrons incident on a thick iron target.

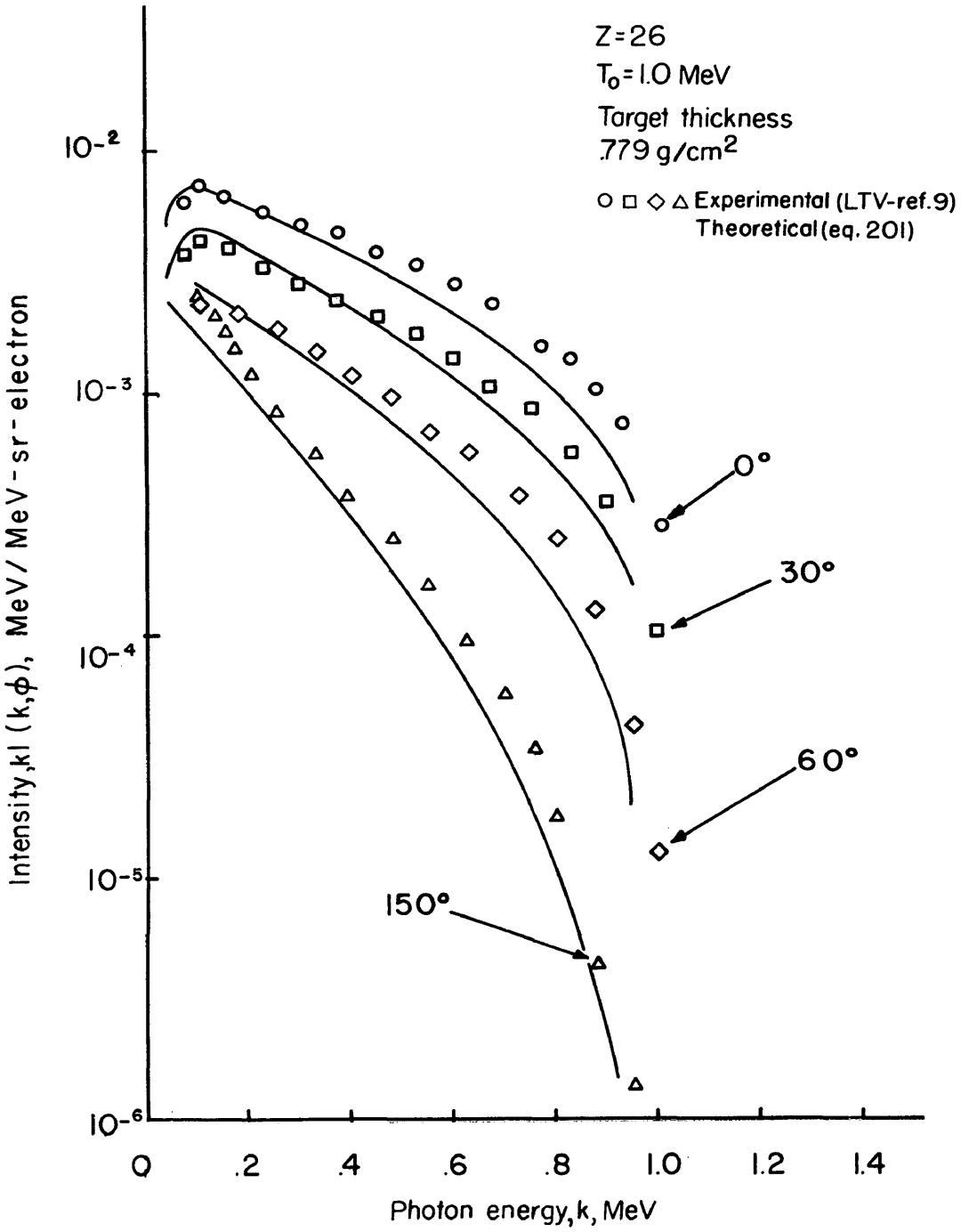

Figure 22. - Comparison of the theoretical and experimental bremsstrahlung spectral intensities at photon angles of 0°, 30°, 60°, and 150° for 1.0 MeV electrons incident on a thick iron target.

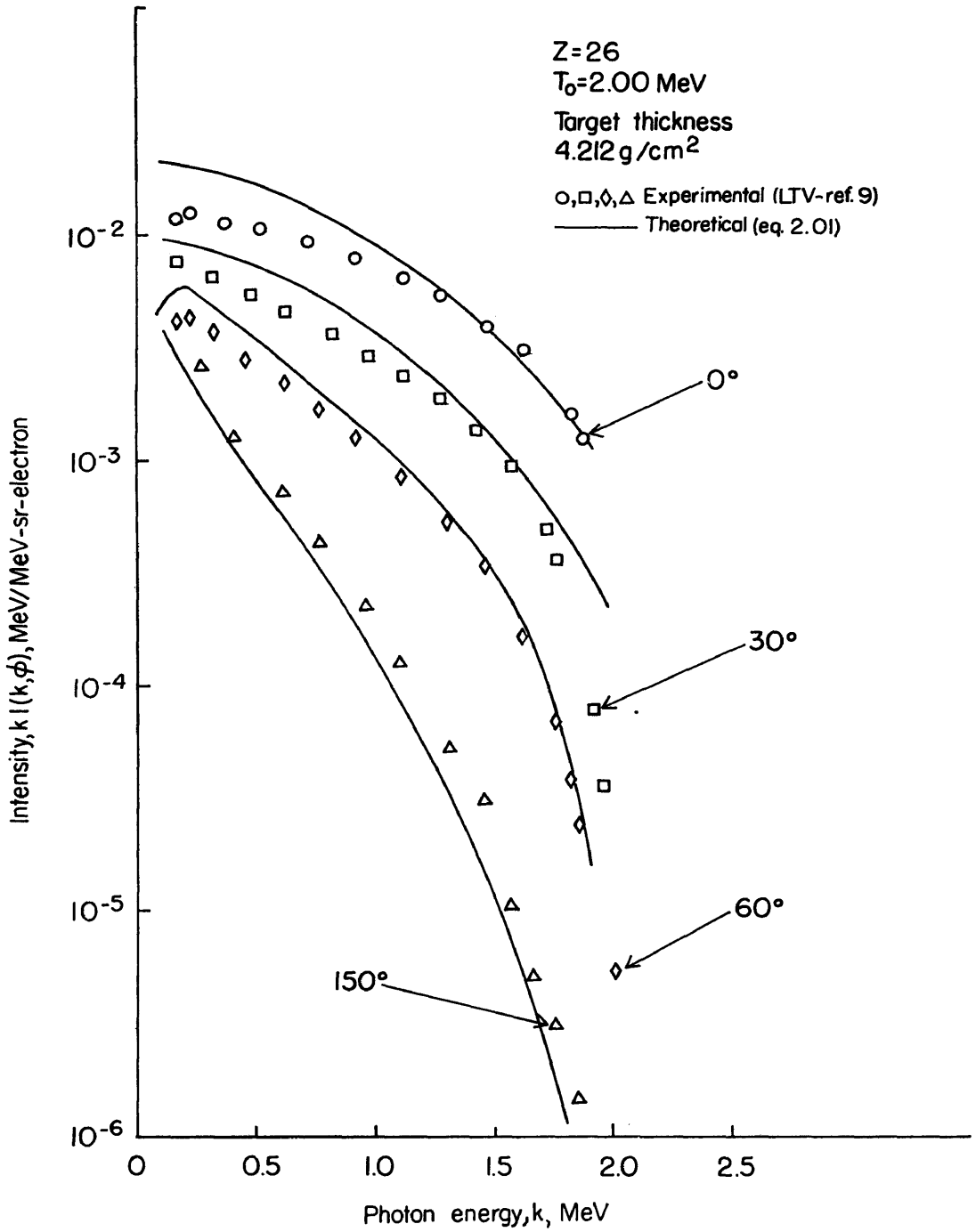

Figure 23. - Comparison of the theoretical and experimental bremsstrahlung spectral intensities at photon angles of 0°, 30°, 60°, and 150° for 2. MeV electrons incident on a thick iron target.

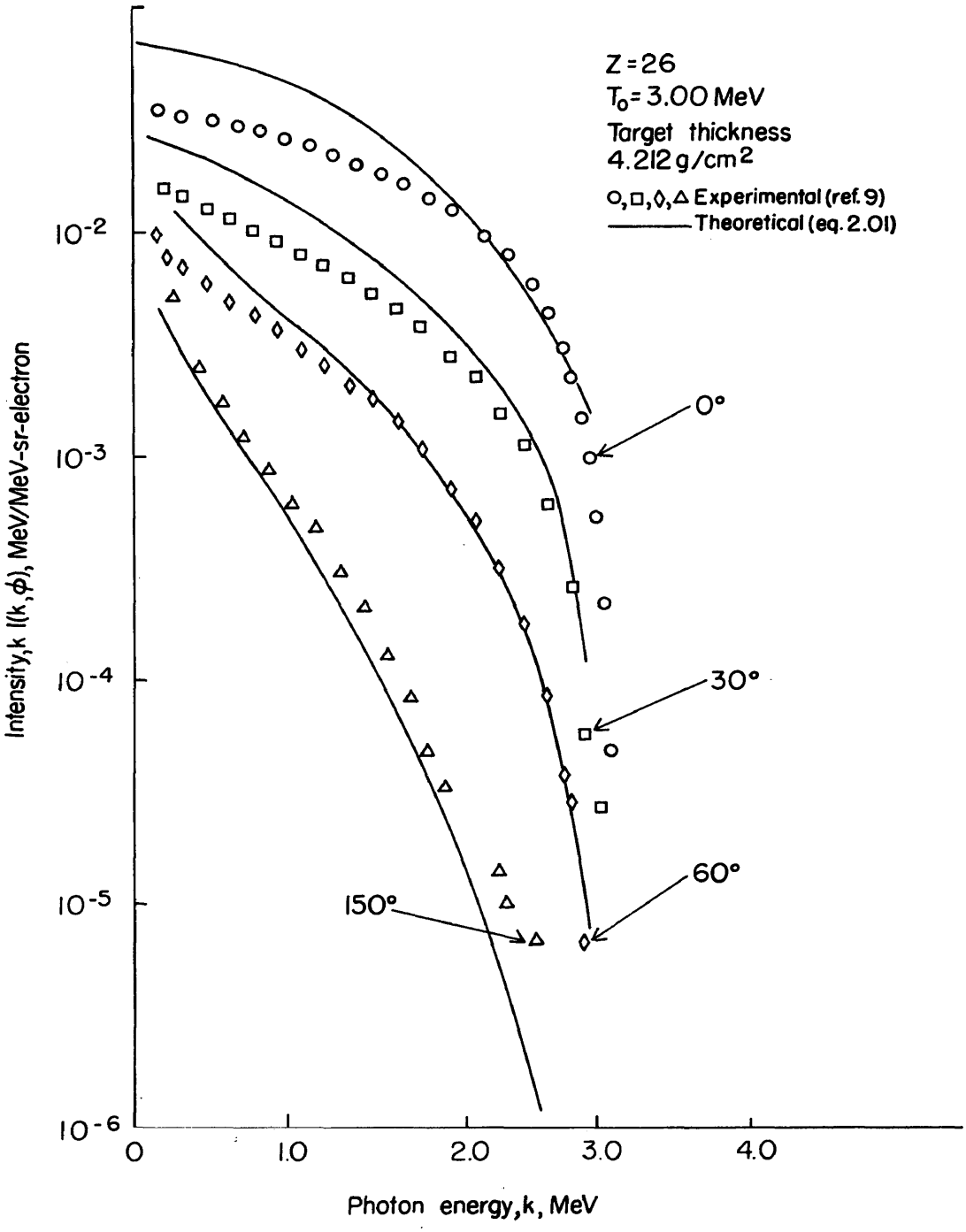

Figure 24. - Comparison of the theoretical and experimental bremsstrahlung spectral intensities at photon angles of 0°, 30°, 60°, and 150° for 3. MeV electrons incident on a thick iron target.

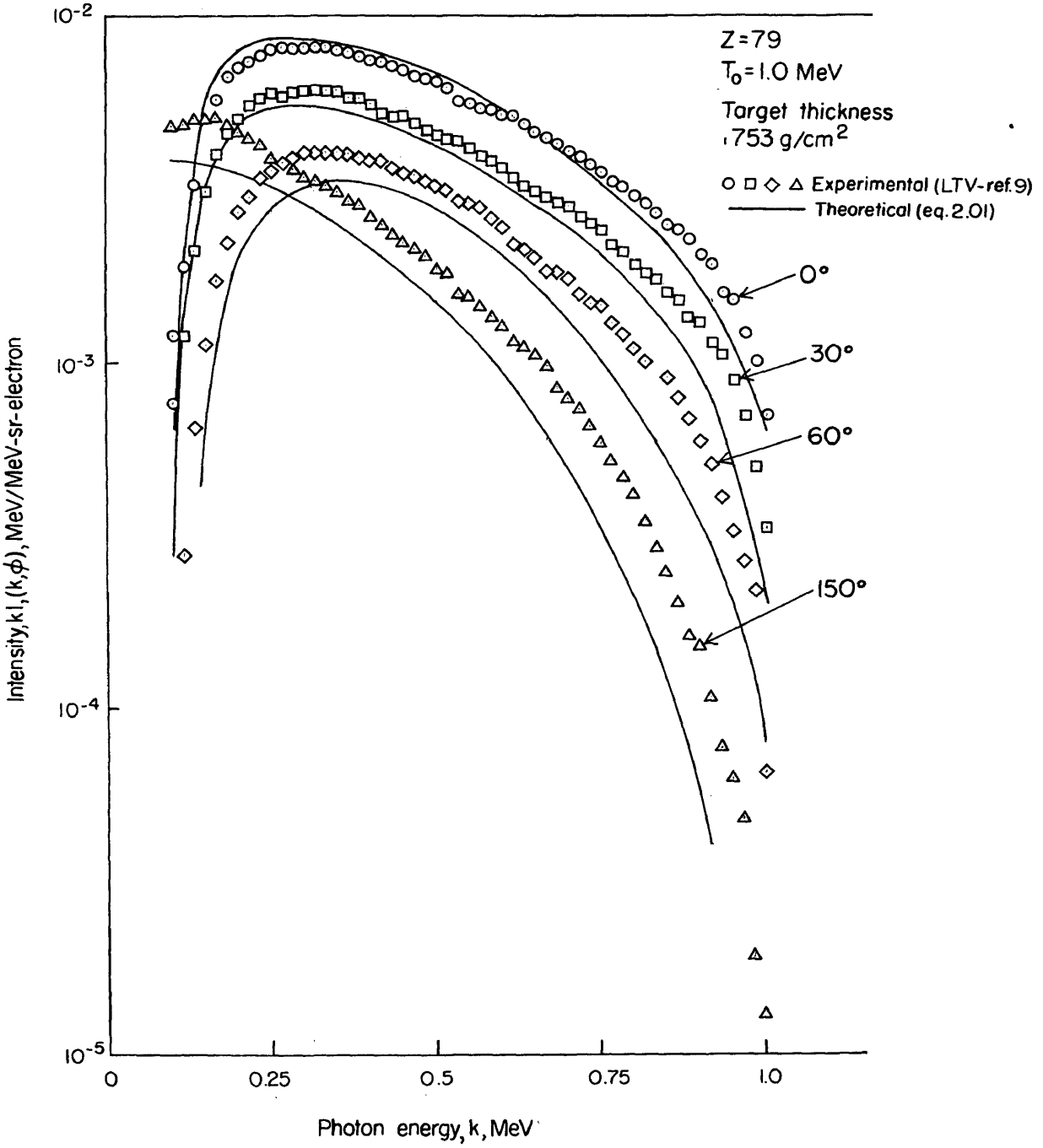

Figure 25. - Comparison of the theoretical and experimental bremsstrahlung spectral intensities at photon angles of 0°, 30°, 60°, and 150° for 1. MeV electrons incident on a thick gold target.

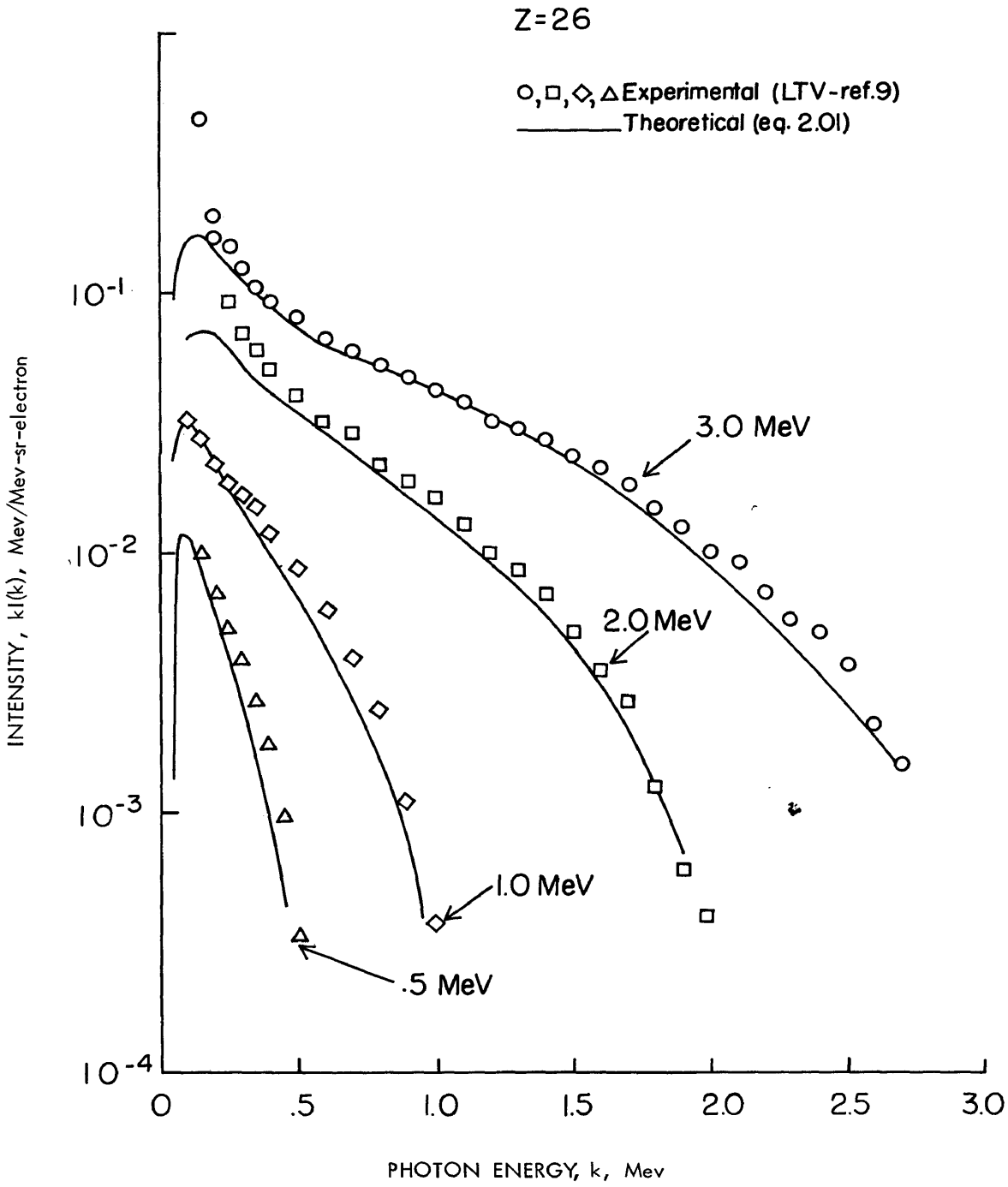

Figure 26. - Comparison of theoretical and experimental photon inten intensities integrated over all photon angles for electron-bremsstrahlung produced by .5, 1.0, 2.0, and 3.0 MeV electrons in thick aluminum targets.

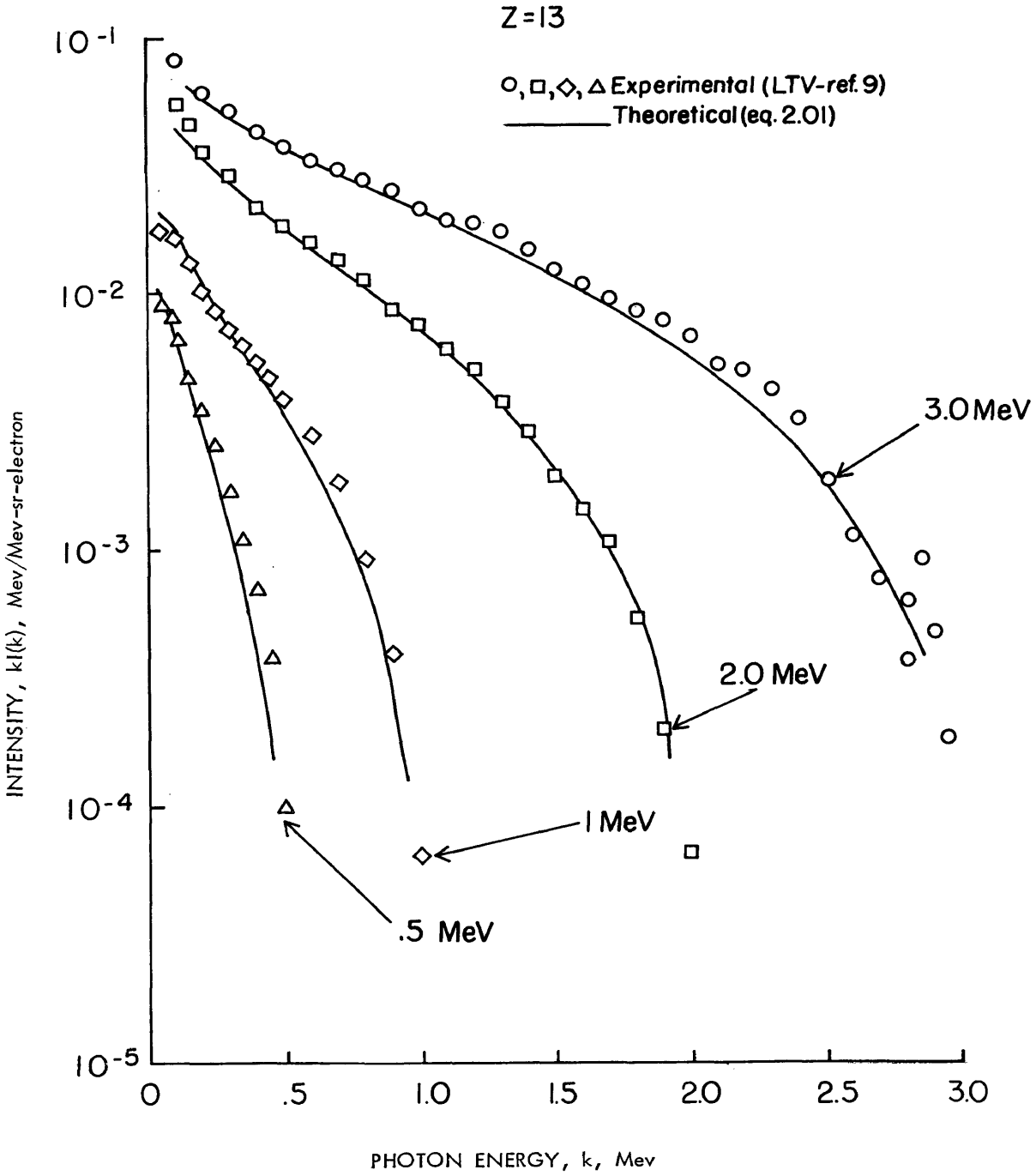

Figure 27. - Comparison of theoretical and experimental photon intensities integrated over all photon angles for electron-bremsstrahlung produced by .5, 1.0, 2.0, and 3.0 MeV electrons in thick iron targets.

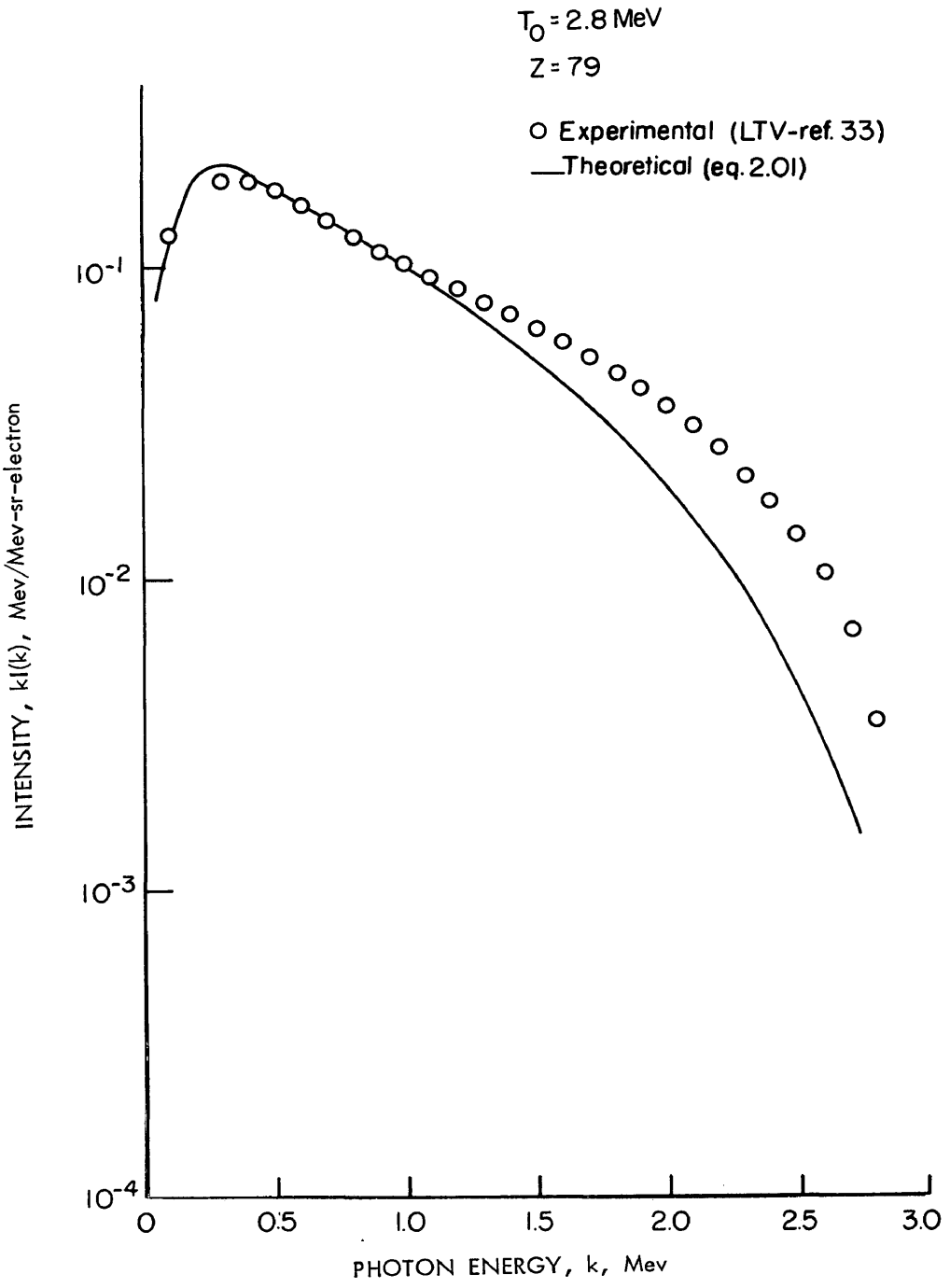

Figure 28. - Comparison of theoretical and experimental photon intensity integrated over all photon angles for electron-bremsstrahlung produced by 2.8 MeV electrons in a thick gold target.

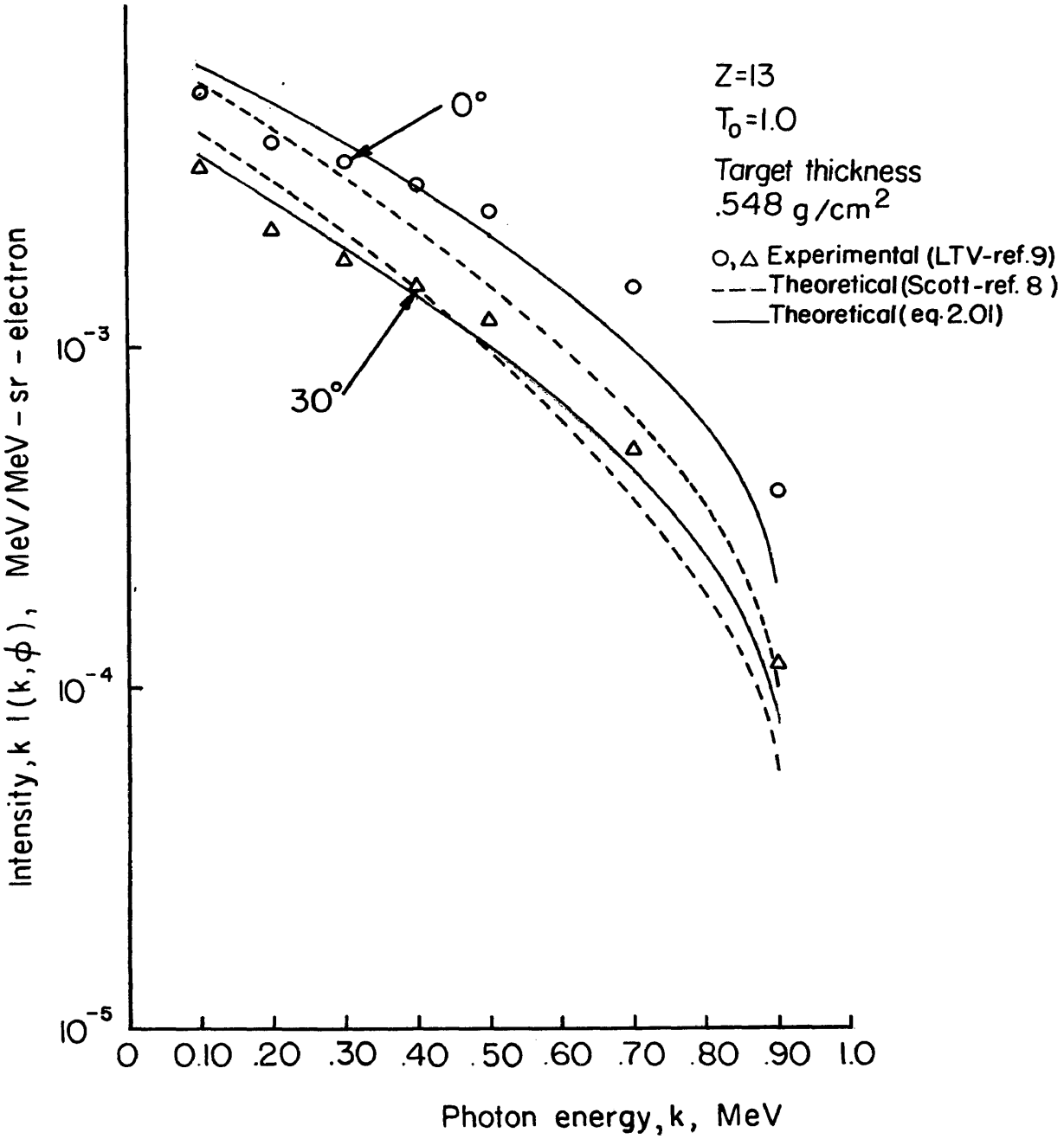

Figure 29. - Comparison of bremsstrahlung spectral intensities calculated from equation (1.05) and equation (2.01) for photon angles of 0° and 30° for 1. MeV electrons incident on a thick aluminum target.

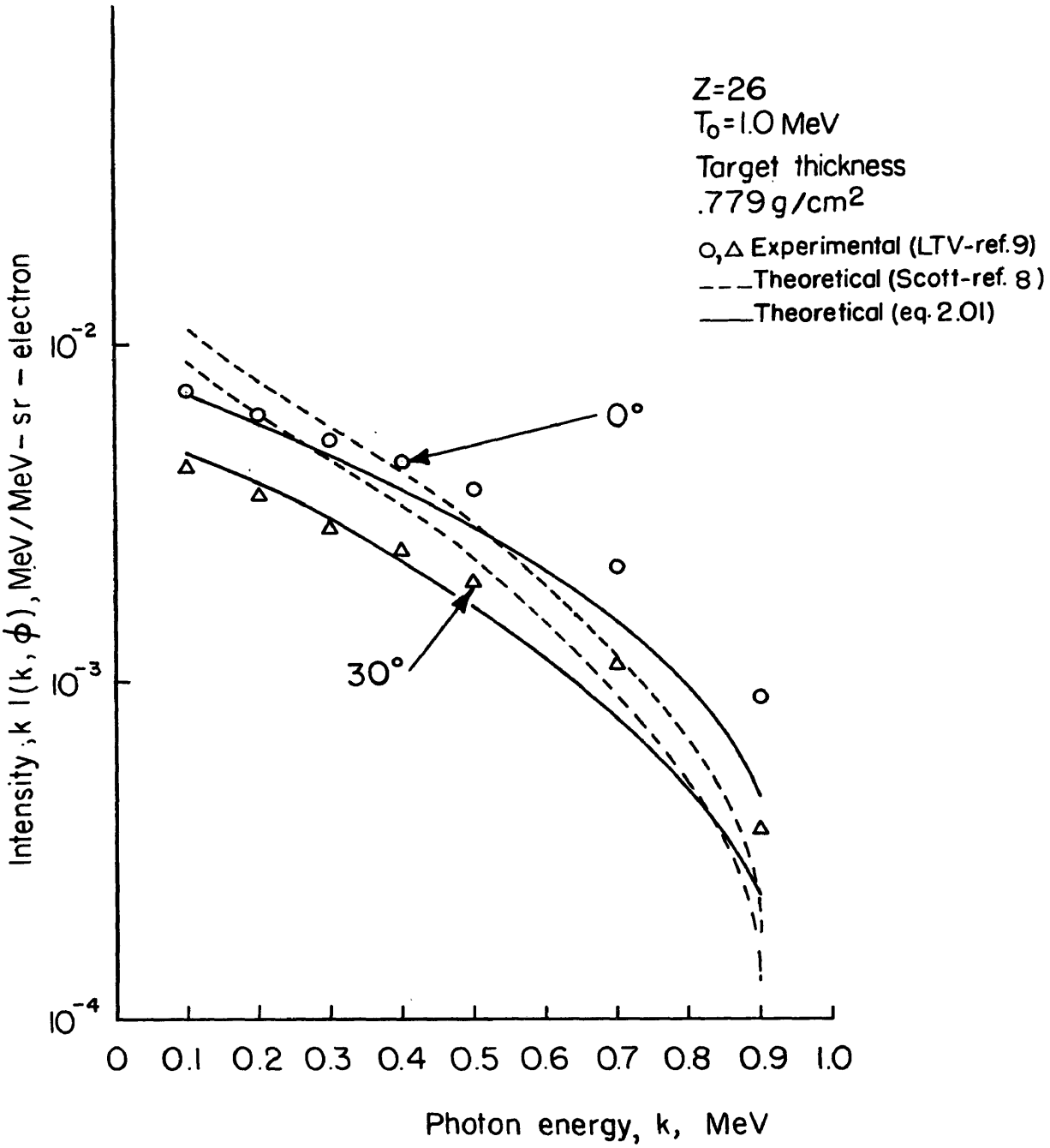

Figure 30. - Comparison of the bremsstrahlung spectral intensities calculated from equation (1.05) and equation (2.01) for photon angles of 0° and 30° for 1. MeV electrons incident on a thick iron target.